NTNU

Norwegian University of
Science and Technology

Fabrication of Diffractive Honeycomb Structures on Silicon Using Photolithography and Maskless Aligner and Investigation of Optical and Electrical Properties of the Structures

Jon Anders Danielsen

Nanotechnology
Submission date: August 2018
Supervisor: Justin Wells, IFY
Co-supervisor: Chang Chuan You, Institutt for Energiteknikk

Norwegian University of Science and Technology
Department of Physics

Preface

The work on this master's thesis was carried out both at the Norwegian University of Science and Technology (NTNU), NanoLab at NTNU, and the Department for Solar Energy at the Institute for Energy Technology (IFE). The general guidelines for the assignement were developed by the co-supervisor Chang Chuan You (IFE) and Sean Erik Foss (IFE), and further adapted by Chang Chuan You when important equipment was unavailable and alternatives had to be found. The work was supervised by Justin Wells (NTNU), who also helped arrange access to equipment at NanoLab.

I would like to thank Justin Wells, Chang Chuan You and Rune Søndenå (IFE) for excellent guidance throughout this thesis work. I would also like to thank the staff at NanoLab, especially Mark Giulio Chiappa (NanoLab), for training and guidance on instruments, in addition to useful discussions. Additionally, I would like to thank all the students in "kull 13" at Nanotechnology, you are all awesome people. Furthermore, The Research Council of Norway is acknowledged for the support to the Norwegian Micro- and Nano-Fabrication Facility, NorFab, project number 245963/F50.

Finally, I would like to thank my family and friends for support and valuable guidance throughout my studies. I would also like to specify that although I have had a lot of help and guidance throughout this work, any errors or shortcomings are my own.

Nesodden,
August 1, 2018

Jon Anders Danielsen

Abstract

Surface texturing is an important method for increasing absorption of light in solar cells. This is done by creating surface structures that increase the optical path-length of photons within the cell, through light-trapping properties. Diffractive honeycomb structures fabricated by laser processing are an example of such texturing methods that have been investigated for use in thin silicon solar cells. A diffractive honeycomb structure is a hexagonal pattern of holes where the feature sizes are roughly the same lengths as the wavelength of visible light.

In this thesis, diffractive honeycomb structures are fabricated by photolithography, using the Maskless Aligner 150 and inductively coupled plasma reactive ion etching (ICP-RIE). Three parameters of the structures are also further investigated; the depth of the holes, the width of the holes, and the coverage ratio of structure to surface area, through the distance between the holes. Light reflection measurements are used to measure the impact of the different parameters on the light harvesting properties of the texture. Additionally, the impact of the surface structures on the electrical properties of the silicon wafer is measured, using photoluminescence (PL) and the quasi-steady state photoconductance (QSSPC) method.

The fabrication of the diffractive honeycomb structures using the Maskless Aligner 150 is considered partially successful. While several samples were fabricated successfully, the method was somewhat unreliable, and the issues that resulted in unsuccessful samples were not clearly identified. The reflection measurements were also affected by the issues in the fabrication method, as some of the samples measured turned out to be unsuccessful samples. For the hole depth measurements, no clear trend could be extracted, but they somewhat indicated that deeper holes have lower reflection. For the hole width measurements, the results indicated a decrease in reflection for hole width lower than 2.5 µm, but no optimal parameter was identified. For the coverage measurements, an overall trend could be seen towards higher coverage ratio resulting in lower reflection values. Lastly, the results from the PL measurements indicated that the diffractive honeycomb structures do affect the electrical properties of the wafer negatively, by lowering the effective lifetime of the minority charge carriers.

Sammendrag

Overflateteksturering er en viktig metode for å øke absorpsjonen av lys i solceller. Dette gjøres ved å lage overflatestrukturer som øker den optiske veilengden til fotoner inne i cellen, gjennom lyshøstingsegenskaper. Diffraktive bikubestrukturer produsert ved hjelp av laserprosessering er et eksempel på slike teksturingsmetoder som har blitt undersøkt for bruk i tynne silisiumsolceller. En diffraktiv bikubestruktur er et heksagonalt mønster av hull der de minste avstandene er på samme størrelsesorden som bølgelengden til synlig lys.

I denne avhandlingen er diffraktive bikubestrukturer produsert med fotolitografi, gjennom bruk av Maskless Aligner 150 og inductively coupled plasma reactive ion etching (ICP-RIE). Tre parametere i strukturen er også videre undersøkt; dybden på hullene, bredden på hullene, og dekningsgrad av struktur mot overflateareal. Lysrefleksjonsmålinger ble brukt til å måle påvirkningen av de forskjellige parameterne på lyshøstingsegenskapene til teksturen. I tillegg ble påvirkningen av overflatestrukturene på de elektriske egenskapene til silisium waferen målt, ved bruk av photoluminescence (PL) og quasi-steady state photoconductive (QSSPC) metoden.

Produksjonen av de diffraktive bikubestrukturene ved bruk av Maskless Aligner 150 regnes som en delvis suksess. Selv om flere prøver ble riktig produsert, var metoden noe upålitelig, og problemene som resulterte i feilproduserte prøver ble ikke tydelig identifisert. Refleksjonsmålingene ble også påvirket av problemene med produksjonsmetoden, da noen av prøvene som ble målt viste seg å være feilproduserte prøver. Fra hulldybdemålingene kunne ingen klar trend oppdages, men de viste en viss indikasjon på at dypere hull har lavere refleksjon. Hullbreddemålingene indikerte en avtagelse i refleksjon for hullbredder mindre enn 2.5 µm, men ingen optimal verdi ble identifisert. Dekningsgradsmålingene viste en generell trend mot at høyere dekningsgrad resulterer i en lavere refleksjon. Avslutningsvis viste resultatene fra PL målingene en indikasjon om at de diffraktive bikubestrukturene påvirker de elektriske egenskapene til waferen negativt, ved å senke den effektive livstiden for minoritetsladningsbærere.

Contents

1 Introduction

This thesis is about recreating and investigating a silicon surface texturing pattern called diffractive honeycomb structure, using photolithography and reactive ion etching. This was done in collaboration with the Institute for Energy Technology (IFE). Diffractive honeycomb structures have been investigated for use on thin silicon wafers by Jostein Thorstensen in his Ph.D thesis "LASER PROCESSING FOR THIN AND HIGHLY EFFICIENT SILICON SOLAR CELLS"[1], and this thesis aims to further investigate some properties of such structures. The original goal of this thesis was to use laser processing to create the surface texture in a somewhat similar way to how the structure was made by Thorstensen, but due to the laser being unavailable, photolithography was chosen as a suitable method instead.

Overall, the objectives of the thesis can be summarized in three goals:

1. Recreate the diffractive honeycomb structure using photolithography, Maskless Aligner, and reactive ion etching.
2. Investigate three parameters of the diffractive honeycomb structure, and find optimal values for these if possible; depth of the holes, width of the holes, and coverage ratio of the holes on the surface. These parameters will be varied across several samples, and their effect on the reflection of the surface will be measured using reflection measurements.
3. Investigate how the diffractive structures affect the surface passivation and the lifetime of the minority charge carriers in the wafer.

Two kinds of wafers were used in this thesis, and detailed descriptions of these can be found in the Appendix, in Tables 3 and 4. An overview of the samples and their relevant procedure parameters can be seen in the Appendix in Tables 5, 6, 7 and 8.

1.1 Motivation

Photovoltaic (PV) power is a rapidly growing source of green energy, as can be seen in Figure 1. This power is generated from sunlight using solar cells. Many research projects aim at further improving PV systems, one of them is the CHEETAH project. Cost-reduction through material optimisation and Higher EnErgy outpuT of solAr pHotovoltaic modules, or CHEETAH for short, is a combined collaborative project, funded under the European Commission's 7th Framework programme. A general goal of the CHEETAH project is "to accelerate the industrialization of innovations", which means working on specific R&D issues, and increase collaboration between R&D providers and industry[2]. This paper falls under one part of the CHEETAH project, focusing on thin wafer solar cells.

Traditionally, silicon wafer production has been focused on using diamond-sawing for cutting mono-crystalline ingots into wafers, and using slurry-based sawing for multi-crystalline

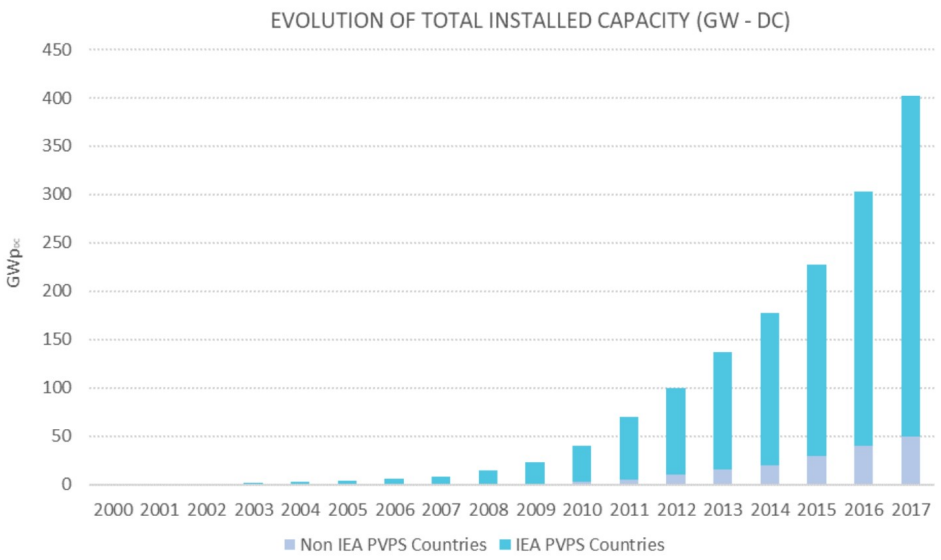

Figure 1: A figure showing the total PV installation capacity worldwide, according to the International Energy Agency[3]

ingots, which inevitably leads to kerf loss, where parts of the ingot are lost as dust during the sawing process[4]. Since the amount of material lost is connected to the number of cuts done, this is not an ideal way of making thin wafers, which increases the number of cuts per ingot. Thus, kerfless methods have been developed for producing thin wafers without loss due to cutting, one of them able to grow wafers between 50 and 250 µm, as explained in a paper by N. Milenkovic et. al.[5]. This poses some challenges for texturing, as less material loss during texturing is acceptable for thin wafers, in addition to the fact that saw-damage is not present, which is used as seeding for isotropic etches in some texturing processes[1]. This problem has been faced before, when transitioning from slurry-based cutting to diamond-wire cutting, as the surface properties after cutting differs significantly between the two methods, making the traditionally used isotropic etching unsuited for surface texturing[4][6]. One of the better alternatives, the random pyramidal structures achieved through etching with KOH, is only viable to <100> surface crystal orientation[1]. This will not work efficiently on multi-crystalline wafers, since they have lots of grains with random crystal orientation, and a new surface texturing method is required for both multi-crystalline wafers and new growing techniques like the one investigated by Ehlers et. al. in their paper "Solution growth of Si on reorganized porous Si foils and on glass substrates"[7], where mainly <111> surface orientation wafers are grown.

1.2 Background

A new method of texturing silicon wafers was investigated by Jostein Thorstensen in the paper "2D periodic gratings by laser processing"[8], as part of his Ph.D thesis work. The

method involved depositing a thin surface layer of silicon nitride, then a novel laser processing step where small 1 µm holes were drilled through the silicon nitride. After this, an isotropic etch was used to create the final structure in the silicon surface, before silicon nitride was removed and the process complete. A monolayer of polystyrene beads was used as micro-lenses in order to increase the spatial resolution of a 515 nm wavelength laser, in the laser processing step. An SEM image of the structure can be seen in Figure 2. The resulting structure was called diffractive honeycomb structure, which was further investigated at IFE. The monolayer of polystyrene beads was exchanged for an array of micro-lenses made of a polymer attached to a quartz glass plate, to be used as a solid mask for the laser. An illustration of the Micro-Lens Array, as it was called, can be seen in Figure 3.

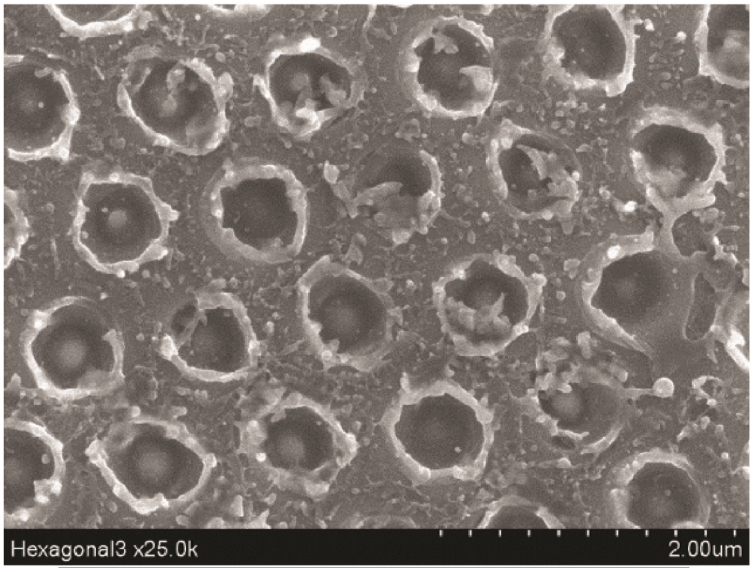

Figure 2: SEM image of the surface structure created by laser irradiation through micro-spheres, presented in Thorstensen's Ph.D[1].

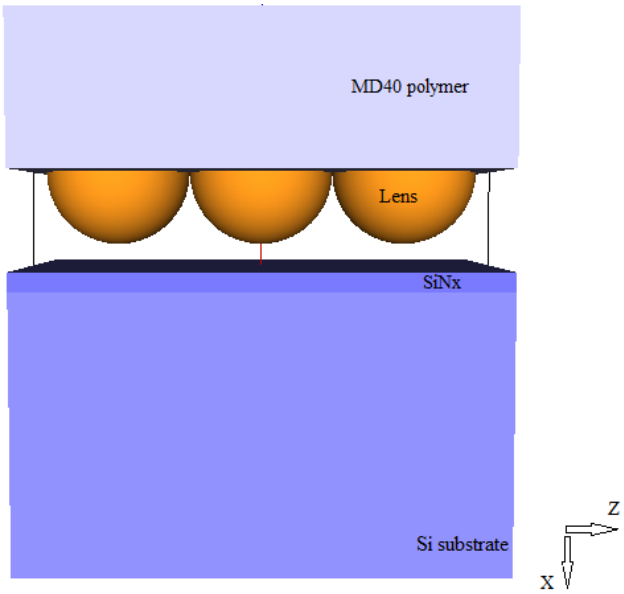

Figure 3: An illustration of the micro-lens array above the sample silicon wafer with a thin surface layer of silicon nitride. Illustration is from an internal memo at IFE.

The entire texturing process with the micro-lens array in mind is illustrated in Figure 4. One of the premises of this process was that a picosecond pulse laser was used, which would do little damage to the silicon wafer and the micro-lens array, compared to lasers with longer pulses. The laser-induced damage was also investigated in Thorstensen's Ph.D [1], and while some damage was discovered, it was concluded that it was possible to mitigate some of that damage through post-process treatments, and that the entire texturing process had potential as an alternative for situations where the pyramidal structure is not useable.

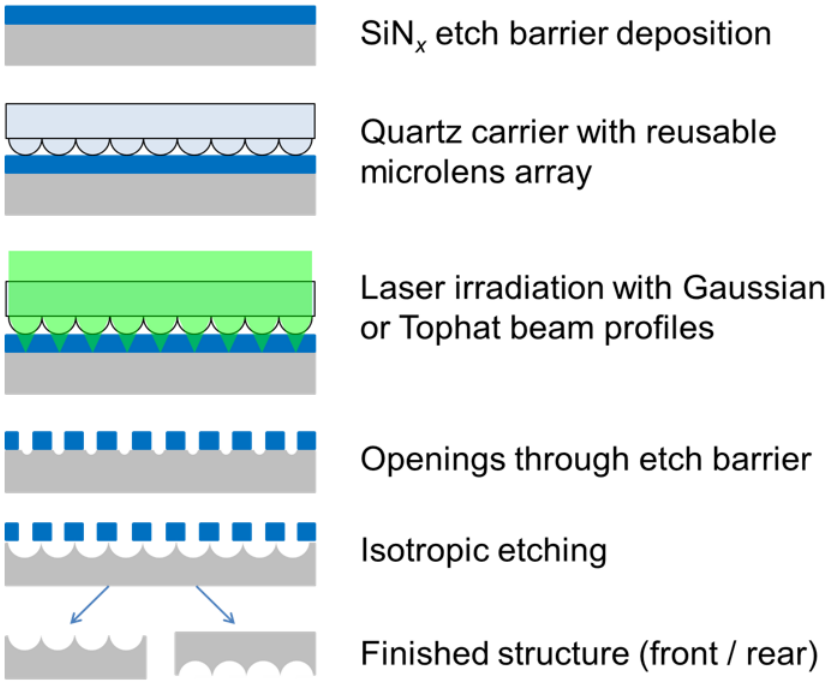

Figure 4: An illustration of different steps during the texturing process when utilizing a picosecond pulse laser and a micro-lens array. Figure is from an internal memo at IFE.

Finally, an image of a well created diffractive honeycomb structure can be seen in Figure 5, where the micro-lens array was used successfully.

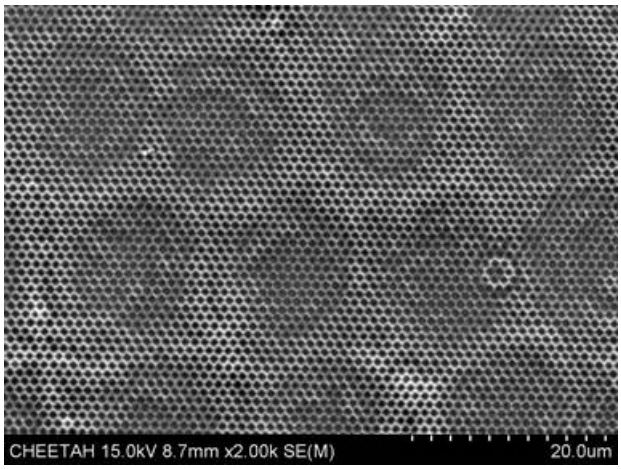

Figure 5: An SEM image of a diffractive honeycomb structure made using a micro-lens array. Image is from an internal memo at IFE.

2 Relevant Background Theory

2.1 Excitation and recombination in semiconductors

Semiconductors, like silicon or germanium, have a bandgap between a valence band full of electrons, and a conduction band with no electrons, when the temperature of the semiconductor is at 0 °K. For realistic temperatures, above 0 °K, a very small fraction of the electrons in the valence band will be excited to the conduction band from thermal energy. This bandgap can be used to create free moving charge carriers, and by exciting an electron from the valence band to the conduction band through absorption of radiation, two charge carriers are created; a negatively charged electron which can move throughout the conduction band, and a positively charged hole which can move throughout the valence band. Since these two charge carriers have opposite charge, they are attracted to each other, and will recombine if they can, releasing radiation upon recombination. Semiconductors can also have their electrical properties altered by introducing dopant atoms with more or fewer valence electrons, thus either adding electrons in the conduction band, or removing electrons from, and thereby creating holes in, the valence band. This is called doping, and adding electrons to the conduction band is called n-doping, and adding holes to the valence band is called p-doping. By the use of a P-N junction, these two charges can be physically separated as well, and the attractive forces, which can be measured as an electrical potential, can be used to force the charge carriers through a closed circuit. This is the simplified working principle of a solar cell, and one of the major challenges to solar cell efficiency is unwanted recombination of charge carriers[9].

Under illumination, the excess charge carrier concentration Δn and Δp in a semiconductor can be described as

$$\Delta n = n - n_0, \tag{1}$$

and

$$\Delta p = p - p_0, \tag{2}$$

for electrons and holes respectively[9]. Here n is the total electron concentration, p is the total hole concentration, and n_0 and p_0 are the respective thermal equilibrium concentrations, meaning the concentrations when not under illumination. The excess charge carrier concentration is also dependent on the intensity of the illumination, with higher intensity leading to higher concentration, and the wavelength of the light, since excitation can only occur when the incoming light has energy equal to or higher than the bandgap energy of the semiconductor.

In p-doped semiconductors, the positive holes in the valence band are called the majority charge carriers, and the electrons in the conduction band are called minority charge carriers. It is the minority charge carriers that supply power from a solar cell, and thus it is important that they do not recombine with the majority charge carriers before they can leave the solar cell through the metal contacts on the surface of the cell. Therefore, the lifetime τ of the

minority charge carriers, the mean time before they recombine, is an important parameter in solar cells. The lifetime τ for minority carriers in a p-doped semiconductor can be described as

$$\tau = \frac{\Delta n}{U}, \tag{3}$$

where U is the recombination rate of the minority carriers. Since surfaces are distinctively different from the bulk of a material[9], an effective lifetime τ_{eff}, is introduced to define the lifetime of a minority charge carrier in a wafer, and can be described as

$$\frac{1}{\tau_{eff}} = \frac{1}{\tau_{bulk}} + \frac{1}{\tau_{surface}}, \tag{4}$$

where τ_{bulk} is the minority carrier lifetime in the bulk material, and $\tau_{surface}$ is the minority carrier lifetime at the surface. However, recombination at the surface of a wafer is usually considered in terms of a surface recombination velocity, S, which in a p-doped semiconductor can be described as

$$S = \frac{U_s}{\Delta n_s}, \tag{5}$$

where Δn_s is the minority carrier excess concentration at the surface, and U_s is the surface recombination rate, given in the units [$\mathrm{cm^{-2}s^{-1}}$]. Assuming the bulk minority carrier lifetime is known, and that the surface recombination rate is equal on both sides of the wafer, the effective surface recombination velocity, S_{eff}, can be estimated from

$$\frac{1}{\tau_{eff}} \approx \frac{1}{\tau_{bulk}} + \frac{2S_{eff}}{W}, \tag{6}$$

where W is the wafer thickness[9]. This approximation does not hold for very high surface recombination velocities, since the diffusion rate for minority carriers through the material will be a limitation as well.

2.2 Wafer thickness and surface textures

Silicon is an indirect bandgap semiconductor, which means that it has a relatively low absorption coefficient compared to direct bandgap semiconductors such as GaAs[10]. When making photovoltaic devices from silicon, the low absorption coefficient affects the light absorption for thin devices. An estimation of this effect can be seen in Figure 6.

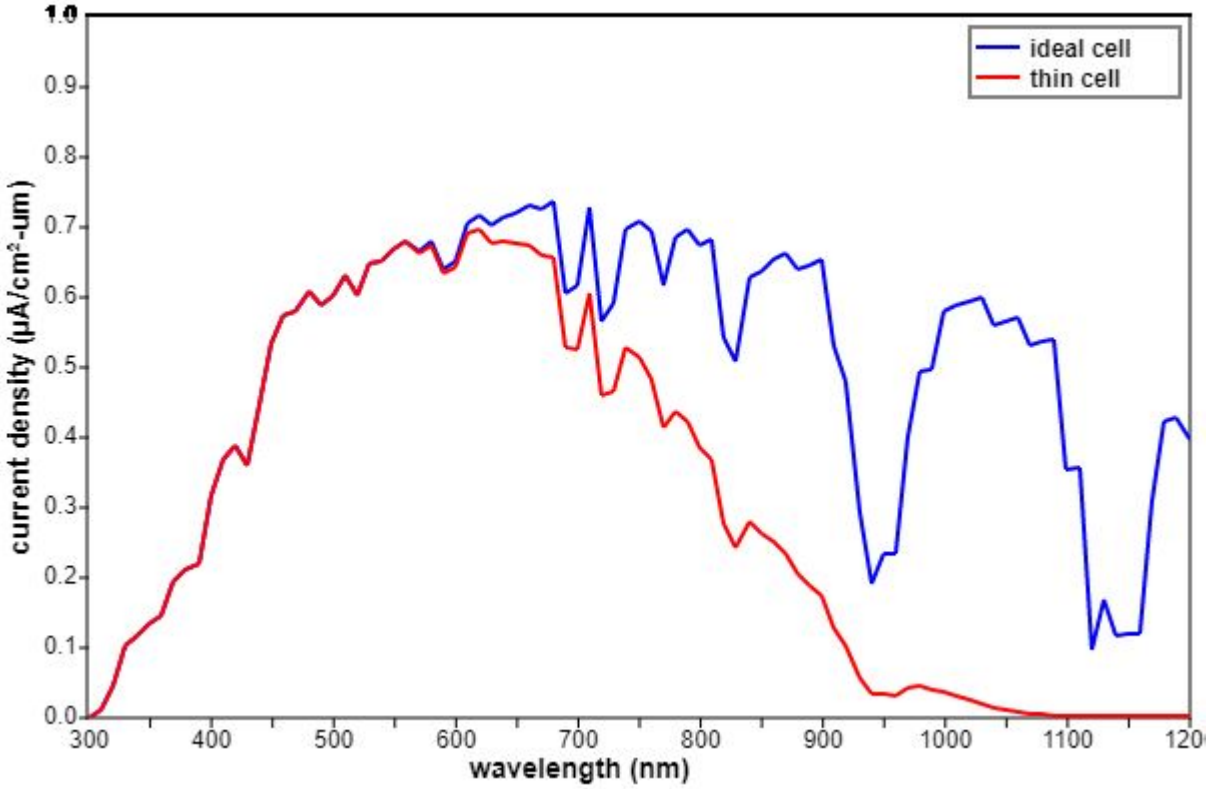

Figure 6: An estimation of the losses in 10 µm thin silicon solar cell, with assumed perfect electronic properties, where the photons only pass through the cell once. Estimation generated at PVeducation.org[11][12].

A way to increase the absorption in a thin solar cell is through light trapping. This is the process of increasing the optical path-length of photons within the cell. This can be done through various techniques, like reflecting the light off of the back surface of the cell, or creating surface textures which makes the incident light come in at an angle instead of perpendicular to the surface. One such method was investigated by Thorstensen et. al. in their paper "Light-Trapping Properties of a Diffractive Honeycomb Structure in Silicon"[13]. In the paper they found that the diffractive honeycomb structure has light trapping properties in between that of the planar and random pyramidal textures, and has potential for use in thin wafer solar cells since it requires no specific surface crystal orientation or seeding from saw damage, and does not cause significant thinning of the wafer.

3 Experimental Method

The experimental work in this thesis was done at Nanolab at NTNU, and at the Sol Department at IFE. For recreating the diffractive honeycomb pattern, there were mainly two options; Electron Beam Lithography (EBL) and photolithography using the Maskless Aligner 150. EBL and photolithography are quite similar techniques, and generally EBL can be described as having higher precision and being more time consuming. Discussions with the staff at NanoLab lead to the decision to use the Maskless Aligner, based on the number of objects in the digital masks that were designed for the thesis, as they typically exceeded tens of millions of objects, which could be an issue for the EBL system to handle.

As for etching the pattern into the surface of the wafer, two relevant options were available; reactive ion etching and wet etching. The process for creating the honeycomb pattern as developed by Thorstensen utilized wet etching[1]. For that to work, a suitable etch barrier needs to be present, which in the original method was a silicon nitride layer drilled through using a laser. In a photolithography method, it would have been somewhat complicated to recreate the silicon nitride etch barrier. In addition, a photoresist was available which was suited as an etch barrier in the reactive ion etching, and that method promised better control of aspect ratio than wet etching, which resulted in photolithography and reactive ion etching being chosen as the methods to create the honeycomb pattern.

3.1 Sample Preparation

Following is a short description of sample preparation relevant to the photolithography method selected. Some shortcuts were used here during the experimental work, based on the assumption that some of the more thorough preparation methods found were meant for making sensitive electrical equipment, and thus unnecessary for the relatively simple structures planned in this project. While this did save time, it might also have affected the results, as discussed in Section 4.1. An overview of the general parameters in the treatment of the different samples can be seen in Appendix, in Tables 5, 6, 7 and 8.

3.1.1 Sample Preparation Theory

If a silicon surface is exposed to air for some time, a surface oxide layer will grow. This grows at a relatively slow rate, of roughly 1 or 2 nm a day[14]. This oxide layer can be an issue if allowed to grow for a long time, into a sizeable surface layer, since that can affect electrical properties at the surface, and thus affect components made from that material[15]. A way to remove the native oxide layer on a silicon wafer, is through etching with HF and water. This will react with the native oxide layer in one of two ways[16];

$$SiO_2 + 4HF \longrightarrow SiF_4 + 2H_2O, \tag{7}$$

or

$$SiO_2 + 6HF \longrightarrow H_2SiF_6 + 2H_2O. \tag{8}$$

The important thing to note here, is that the chemicals will not react with the bulk silicon, and thus clean the surface of native oxide without further affecting the surface, which makes it a suitable cleaning etch to do before experimenting with silicon wafers.

When it comes to cleaning and preparing a silicon wafer for experiments, a general cleaning procedure has been compiled by the University of California, which include the following steps[17]:

1. Solvent clean, for removing oils and organic residues.
2. RCA clean, for removing organic residues, and creating a small surface oxide layer.
3. HF-dip, for removing any surface oxide layer.
4. DI water cleaning and blow drying with nitrogen, to remove any remaining chemicals on the surface.

3.1.2 Procedures followed

There were two kinds of wafers used in the experiments. One was from Siegert Wafer, a p-type wafer with surface orientation <100>, a thickness at about 275 µm, and a diameter of about 100 mm. This wafer type was used for all samples but the lifetime samples. The second kind of wafers was a float-zone p-type wafer from Topsil, with surface orientation <100>, thickness of about 275 µm, and size at about 100 mm. Details on the wafers used can be seen in the Appendix, in Tables 3 and 4.

Two sample sizes were used in the experiment, based on the requirements from characterization instruments. The most numerous samples were 15 mm by 15 mm squares, which were meant for reflection measurements, while a few samples were 35 mm by 35 mm squares, meant for minority carrier lifetime measurements.

When choosing the cleaning procedure to follow in the experiment, it was decided that the compiled cleaning procedure from the University of California was a bit too comprehensive, and thus it was shortened a bit. The sample cleaning procedure used in the experiments was as follows:

1. Solvent clean; samples were cleaned using acetone, then ethanol, then DI water.
2. HF-dip; samples were submerged in 5 % HF (95 % water) for 2 minutes, then cleaned with DI water, and then blow-dried with nitrogen gas.
3. Another solvent clean; acetone, ethanol, water, followed by blow-drying with nitrogen.

The reason for the last solvent clean was that in some cases, there were several days between the HF-dip and the experiments, and since solvent cleans are fast and simple, they were always performed before applying photoresist. New HF-dips after a few days of air-exposure were deemed unnecessary, as it was assumed the thin layer of oxide formed in a few days would not affect the experiments significantly, since the measurement techniques used were not very surface sensitive. This, combined with the reduced cleaning procedure, might have been the cause behind some of the problems described in Section 4.1.

3.2 Photoresist

3.2.1 Photoresist Theory and methods chosen

Photoresists are light-sensitive materials, that can form or break polymer chains when exposed to light with certain wavelengths. There are two general types of photoresist, referred to as positive and negative resists, and the difference between the two is how they react to the light. A positive photoresist will react to the light by breaking polymer chains, making the exposed parts of the resist weaker, which will make it possible to dissolve the exposed part without dissolving the unexposed part, with the right developer. The opposite happens in a negative photoresist, meaning that polymer chains are formed due to reactions with the light[18]. This is illustrated in Figure 7.

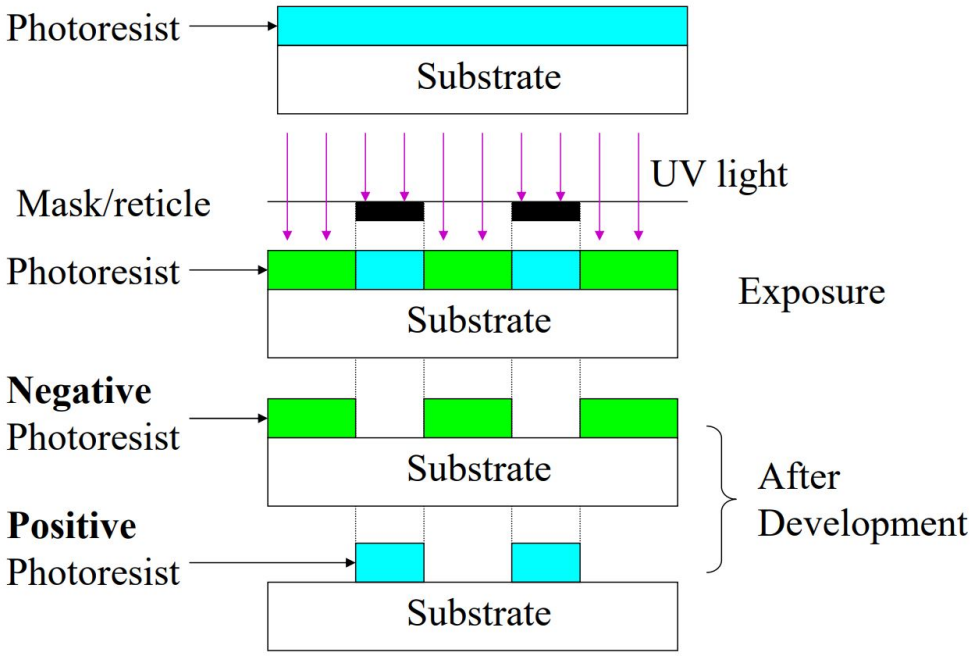

Figure 7: An illustration of the difference between a positive and a negative photoresist[19].

The photoresist chosen for the experiment was the positive resist MEGAPOSIT SPR 700, mainly because it worked well with the Maskless Aligner 150 and the reactive ion etching, according to the staff at NanoLab. Additionally, the design masks made for this project often contained tens of millions of objects, but they still only covered a small part of the surface, usually less than 20 % of the surface area. Since a positive photoresist only needs to illuminate the parts that are to be dissolved by the developer, an assumption was made that the Maskless Aligner would work faster with a positive resist, since less of the surface would then need to be exposed. This assumption was later proved wrong, as the Maskless Aligner 150 exposes at the same speed regardless of the number of objects or surface fraction to be exposed, which meant that negative photoresists could also be used without extending exposure time.

Applying a photoresist and creating a suitable etching mask on a wafer can be described as a ten-step process[18], and following are short descriptions of the ten steps and how they were executed (described as the method):

1. Cleaning the wafer; usually involves using solvents, but can also include plasma etches, acid dips, etc.

   Method: HF-dip for 2 minutes to remove the native oxide layer, then cleaning using acetone, ethanol and finally De-Ionized (DI) water.

2. Dehydration bake; heating the wafer on a hot plate to remove liquids from the surface, usually water, as that is usually the last chemical used in the cleaning process.

   Method: Dehydration bake was done on a hot plate at 180 °C for 5 minutes. After this, the wafers were cooled on a cold plate, at roughly room temperature, for 5 minutes or more.

3. Applying a primer; this is a chemical meant to increase the adhesiveness of the surface, making the photoresist stick better to the surface.

   Method: A Primer was not applied, as it was deemed unnecessary for the structures created and methods used in this project. This was partly due to the fact that primers were not widely used by practiced users of the photolithography equipment at NanoLab.

4. Applying photoresist; usually done by applying a puddle of liquid photoresist on the sample, then spinning the sample to create an even and thin layer. The acceleration, spin speed and spin time are important parameters which affect the resulting surface layer.

   Method: The photoresist was applied evenly on the entire surface, wasting some photoresist compared to only a puddle in the middle of the sample surface. This was done after several films did not cover the sample after spinning when applying only a puddle. The parameters chosen were an acceleration of 4000 RPM/s for 1 s, then spinning at 4000 RPM for 30 seconds. This was a commonly used program for the SPR 700 photoresist, aimed at a layer thickness of about 1 µm, which also fit the spin

speed curve in the user guide for the photoresist[20].

5. Soft bake; a mandatory step defined by the producer of the photoresist. This is used to remove most of the solvent in a liquid photoresist, turning it into a solid film on the surface of the wafer.

   Method: Soft bake was done at 95 °C for 1 minute, as recommended by the photoresist producer[20].

6. Exposure; exposing parts of the photoresist in order to create the desired structure. The exposure dose, meaning the amount of energy irradiated at the photoresist, affects the resulting structure. Factors which affect how large the exposure dose should be, include the thickness of the photoresist, and the kind of walls wanted on the structure. It is normal to test different exposure doses for specific structures, in order to identify what dose leads to the optimal result.

   Method: After exposure dose testing, 125 mJ/cm^2 was chosen as the exposure dose to be used for all samples. This was based on both microscope and SEM images, but it is possible that the ideal exposure dose was not identified correctly. Some of the images used in this task can be seen in the Appendix, in Section 6.

7. Post exposure bake; another bake on hotplate, which is usually required, depending on the photoresist used.

   Method: Post exposure bake was done at 115 °C for 1 minute, as recommended by the manual[20].

8. Development; samples are dipped in a developer for a set amount of time, which dissolves parts of the photoresist, creating the structure on the surface.

   Method: Megaposit developer MF-26 A was used, which was not the one recommended by the manual, but it was a good replacement with similar properties, according to the staff at NanoLab. The samples were dipped for 1 minute, as recommended by the manual. For the small samples, the samples were shaken during the development, because several of the early samples did not develop fully when only submerged. The larger samples were held still while submerged, as the adhesion of the photoresist layer was weaker, and the layer often was entirely removed during development when shaking.

9. Development inspection; the developed structures are inspected, usually with a simple light microscope, to ensure good development.

   Method: A light microscope was used to inspect the photoresist after development. Too often this step would reveal that the development did not go as planned, and the photoresist layer would have to be remade. Whenever that was the case, the samples went through the last solvent clean step described in Section 3.1.2, before the photolithography process was restarted.

10. Hard bake; this step is optional, and usually only done for photoresist which is meant to act as an etch barrier. The hard bake is another step which is described by the producer of the photoresist.

    Method: Hard bake was done at 130 °C for 3 minutes, followed by cooling at a cold plate for 3 minutes.

3.3 Maskless Aligner 150

The Maskless Aligner 150 was chosen for recreating the diffractive honeycomb structure in this project. The reasons why this was chosen are described in Section 3, but in summary it was because the laser system at IFE was unavailable, and EBL was not suitable for the number of structures to be created. The Maskless Aligner is an instrument manufactured by Heidelberg Instruments, and it is meant as a replacement and improvement to traditional contact-mask systems used in photolithography, by using mirrors and lenses to only expose certain areas of the samples, instead of using a physical mask to stop the radiation from hitting those areas. The software converts a number of different design file formats to the format used by the machine, and then exposes the areas designated by the mask. The wavelength of the light used in the experiment was 405 nm, which is at the lower edge of the visible spectrum. This wavelength was chosen to fit the photoresist, out of the available wavelenghts in the instrument. The producers especially advertise the fast exposure time, where a 50 mm x 50 mm surface can be exposed in 4 minutes irrespective of the number of structures or the fill factor[21].

3.3.1 Digital Mask design

The masks were designed using a program called CleWin4, and the format used for the files were .gsdii. The reason this format was chosen over other formats like the .dfx, was that it had a significantly smaller file size. A typical file size for a mask with 50 million objects was at tens of KB, while the same mask would be several GB in the .dxf format. This is interesting, because it might have had a large effect on the conversion time, which could become quite excessive. The total time for the exposure process was at about 1 minute per 1 million objects in the masks, which meant that the largest masks at about 150 million objects took about two and a half hours to expose, and that a few masks with several billion objects were simply not feasible and were therefore never used. When considering the statement from the producer that the exposure time is irrespective of the number of structures[21], it seems likely that the conversion is to blame for the delay, and it is therefore possible that using the flat-structure .dxf file format might have been significantly faster in conversion than the .gsdii format. An example of a mask used can be seen in Figure 8. Since this hexagonal pattern is common for all masks used in the thesis, the only difference between the masks are two distances; hole diameter and distance between holes. An overview of the

distances and diameters used can be seen in Tables 5, 6, 7 and 8.

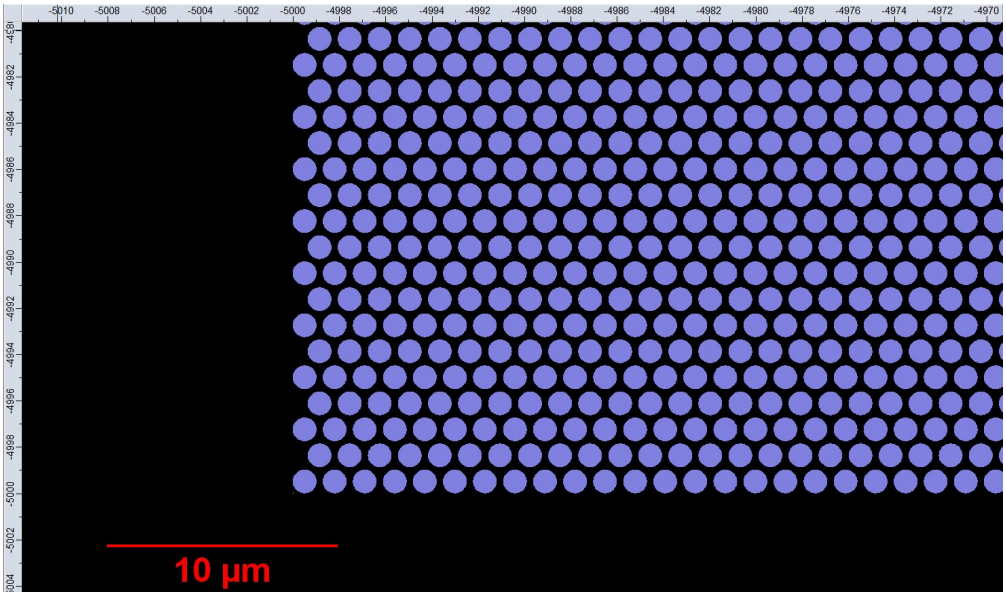

Figure 8: An image of a small part of a mask used in the Maskless Aligner. The distance between the holes is 300 nm, while the hole diameter is 1 µm.

3.4 Reactive Ion Etching

For the etching done in this experiment, Inductively Coupled Plasma - Reactive Ion Etching (ICP-RIE) was chosen.

3.4.1 Etching Theory

The ICP-RIE etches a surface with two main mechanics; a physical etch where ions from a plasma bombard the surface, and a chemical etch where the bombarding ions react with the surface. An illustration of the working principles of the ICP-RIE can be seen in Figure 9. The key feature to note is the ability to control both the ICP generator power, and the bias generator power, in addition to the chemicals used in the plasma, which gives a large process window where ion current, ion energy and ion species can be determined by the user[22].

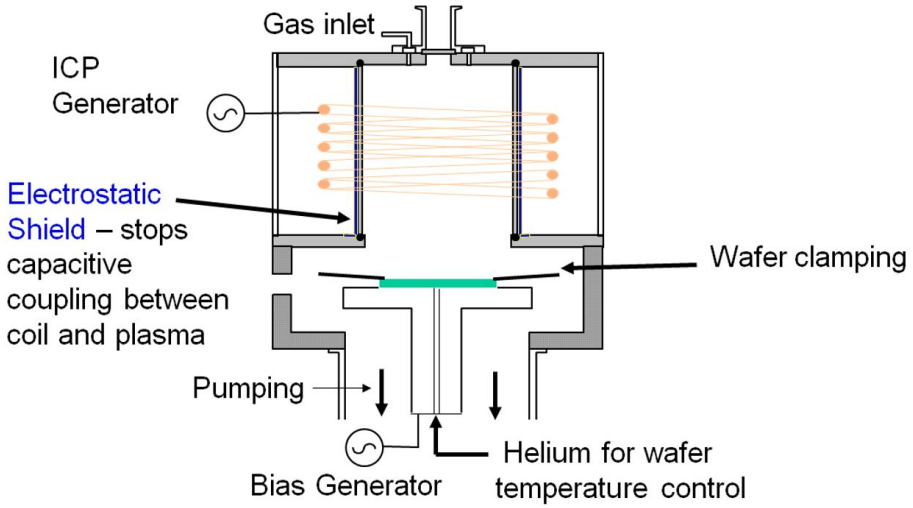

Figure 9: An illustration of the working principles of the ICP-RIE, from the ICP-RIE Chiller Short Guide at NanoLab[23]. The entire process is done in low vacuum, typically around 1-90 mTorr.

3.4.2 Chosen parameters

As editing and programming new processes in the ICP-RIE is a considerable effort, which requires experience on the instrument, an already existing program for etching silicon, made by an experienced user at NanoLab, was used with permission for the etching step. The details of the parameters used are given in the Appendix, in Table 9. The only varying parameter for this project was the etching time, which was varied for the hole depth investigation. The etching times used for the hole depth samples were 30, 60, 90, 120, 150, and 180 seconds, as seen in Table 5. These parameters were chosen based on an etching test where the etching rate for the silicon was found to be roughly 300 nm per minute.

3.5 SEM analysis

Scanning Electron Microscopy is a surface imaging technique that works on the principle of accelerating electrons using high voltages, and then directing them towards the surface of a sample. By utilizing the resulting short wavelengths of the electrons, the electron beam can be focused on a very small area of the sample. The electrons crash into the sample at high velocity, and can both excite electrons which escape from atoms at the surface, called secondary electrons, or be scattered back from collisions with heavier elements at the surface or a short depth into the sample, called backscattered electrons. The SEM can be set to detect either backscattered or secondary electrons, and create an image of the sample surface from the detection pattern. The beam scans over a section of the sample surface [24].

Some cross-section images were taken, and this was done by scribing samples roughly in half, and then mounting half a sample at a tilted sample holder.

3.5.1 Instrument used

The instrument used to take the SEM images was the FEI APREO at NanoLab.

3.6 AFM analysis

Atomic force microscopy is another surface imaging technique, where a probe scans over the surface and the position of the probe is measured while scanning. The probe usually consists of a cantilever, with a small tip on the edge that scans along the sample. A laser is reflected off of the cantilever towards a detector which can detect movement in both X and Y direction, which is used to determine the position of the probe on the sample[25]. An illustration of an AFM set-up can be seen in Figure 10.

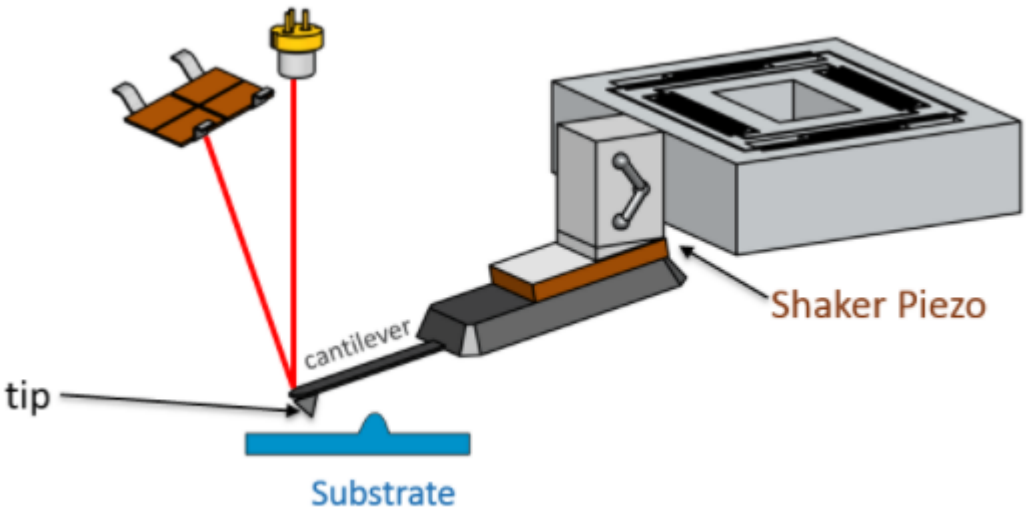

Figure 10: An illustration of the working principle for the AFM. Figure taken from educational material from Nanosurf[25].

3.6.1 Instrument used

The AFM images were taken with an AFM Veeco diMultimode V, which can be seen in Figure 11.

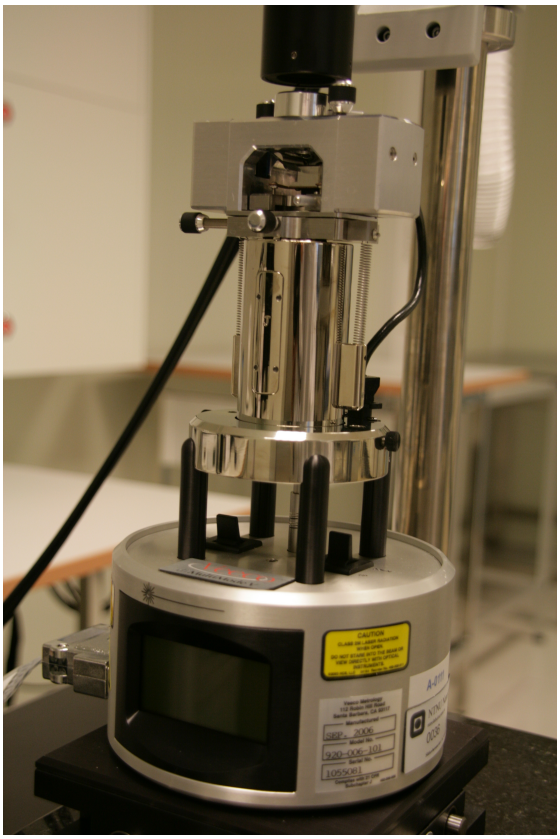

Figure 11: The AFM used in the experimental work.

3.7 Reflection measurements

This technique focuses on how electromagnetic radiation within the visible spectrum interacts with a sample. One way to use this technique is to shine a light on the surface of a sample, and measure the intensity of the reflected wavelengths. Reflection measurements were used in this project to determine how effective the diffractive honeycomb structures were at scattering incoming light.

3.7.1 Instrument used

The instrument used in this project is from the line of Ocean Optics Spectrometers. Ocean Optics Spectrometers measure reflection by sending the reflected light through a grating, which spatially separates the wavelengths linearly perpendicular to the slits in the grating. The separated wavelengths are afterwards directed towards a linear CCD detector[26]. An illustration of the principle can be seen in Figure 12. The set-up used in the reflection measurements is shown in Figure 13, with a light trap mounted instead of a sample. The

light trap was used as a reference for no reflection, and a pyramidal textured Si wafer was used as a reference value between each use of the instrument.

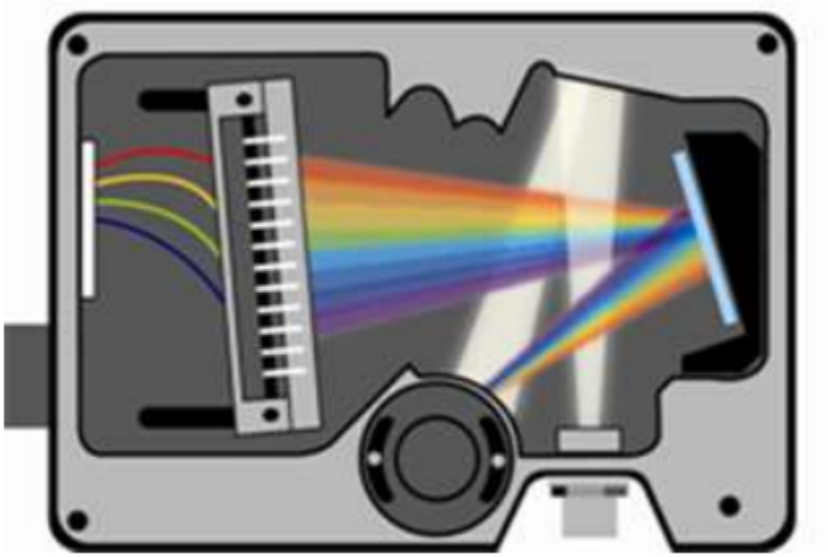

Figure 12: An illustration of the working principle of the Ocean Optics Spectrometer series. Figure taken from Ocean Optics educational material[26].

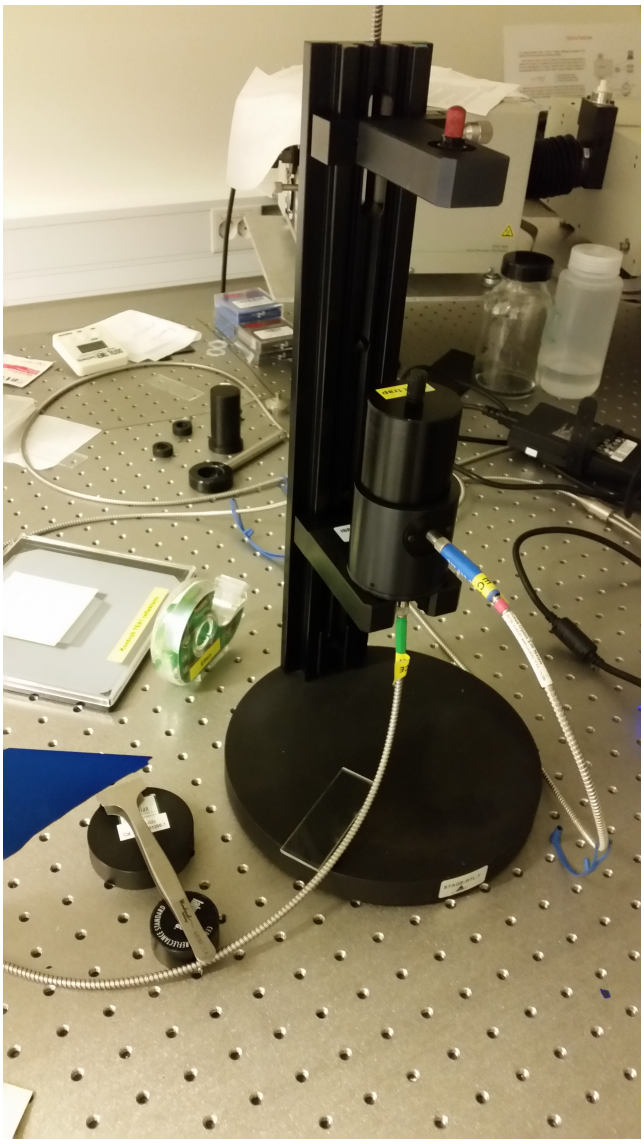

Figure 13: Setup used for reflection measurements, here seen with a light trap mounted instead of a sample.

3.8 Surface Passivation

Surface passivation is a wide description of techniques used to reduce the surface recombination rate in solar cells. There are many different ways to reduce surface recombination, and some of them include adding a passivating layer on the top and bottom of the wafer. For the lifetime measurements, a passivation layer was needed before lifetime could be measured. Plasma Enhanced Chemical Vapor Deposition (PECVD) was used to deposit a layer of amorphous silicon and a layer of silicon nitride, called an α-Si:H / SiNx stack, and this

was done at IFE. The experimental details of the passivation process will not be presented in this thesis, as they are part of a confidential passivation technique developed at IFE.

3.8.1 Process details

Before passivation, all lifetime samples were etched in HF to remove any native oxide on the surface, and to clean the samples. There were four samples meant for lifetime measurements, which were all processed simultaneously in the PECVD process. Of the four samples, two of them had the diffractive honeycomb structure etched into the surface, but with different feature sizes, a third was etched without any structure at all as a reference for the damage induced by the etching, and a fourth sample was completely untreated before the passivation, to serve as a reference of the lifetime in an untreated wafer.

Unfortunately, the process chamber of the PECVD instrument was not cleaned properly before the process. A normal pre-conditioning was run, which in normal circumstances would have been sufficient, but the machine had been through maintenance earlier that week, which apparently could leave large amounts of dust and metal particles in the reaction chamber. It is possible that this had an adverse effect on the lifetime measurements of the samples. While the samples could have been remade, this was not done due to time constraints.

3.9 Lifetime measurements

Lifetime measurements were done using the Quasi-Steady State Photo Conductance (QSSPC) method in a photoluminescence (PL) imaging system (model LIS-R1) from BTImaging[27]. Some lifetime background theory can be found in Section 2.1

3.9.1 QSSPC theory

The QSSPC method measures the effective minority carrier lifetime, τ_{eff}, as a function of the minority excess carrier concentration, Δn in a p-doped semiconductor or Δp in an n-doped semiconductor[28]. It does this by measuring both the conductance and the photogeneration of the sample under steady-state illumination. The conductance, σ of the wafer under illumination can be described as

$$\sigma = q\Delta nW(\mu_n + \mu_p), \tag{9}$$

where q is the charge of the electron charge, and μ_n and μ_p are the electron and hole mobility respectively. Using an inductive coil connected to a Radio Frequency bridge, the conductance of the sample can be measured while under illumination. Next, the photogeneration rate,

$J_{generation}$, under steady-state conditions is equal to the recombination rate, $J_{recombination}$, of the sample, and can be described as

$$J_{generation} = J_{recombination} = \frac{q\Delta nW}{\tau_{eff}}. \tag{10}$$

This photogeneration is measured relative to a calibrated photo diode, and with both the photogeneration and conduction measured, and assuming bulk mobility values for the material is known, the effective lifetime can be described as

$$\tau_{eff} = \frac{\sigma}{J_{generation}(\mu_n + \mu_p)}. \tag{11}$$

An illustration of the working principles behind a QSSPC measuring instrument can be seen in Figure 14.

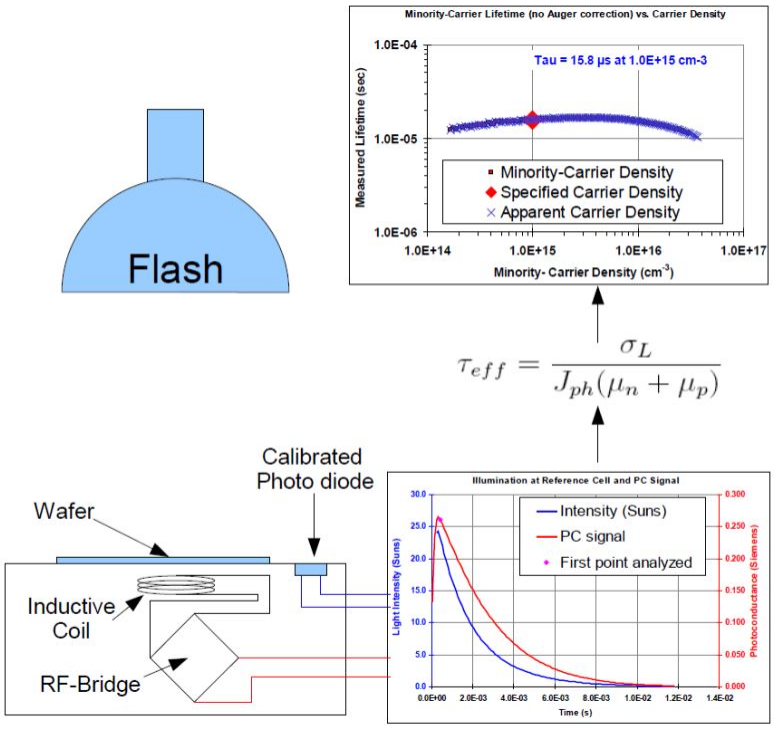

Figure 14: An illustration of the QSSPC setup[29], as presented in Susanne Hellands master thesis[30].

4 Results and Discussion

4.1 Pattern Recreation

The first goal of the project was to recreate the honeycomb texture using the Maskless Aligner. Several issues were faced in trying to recreate this pattern, and the biggest challenge was loss of adhesion for the patterned photoresist to the wafer surface during development, as can be seen in Figure 15.

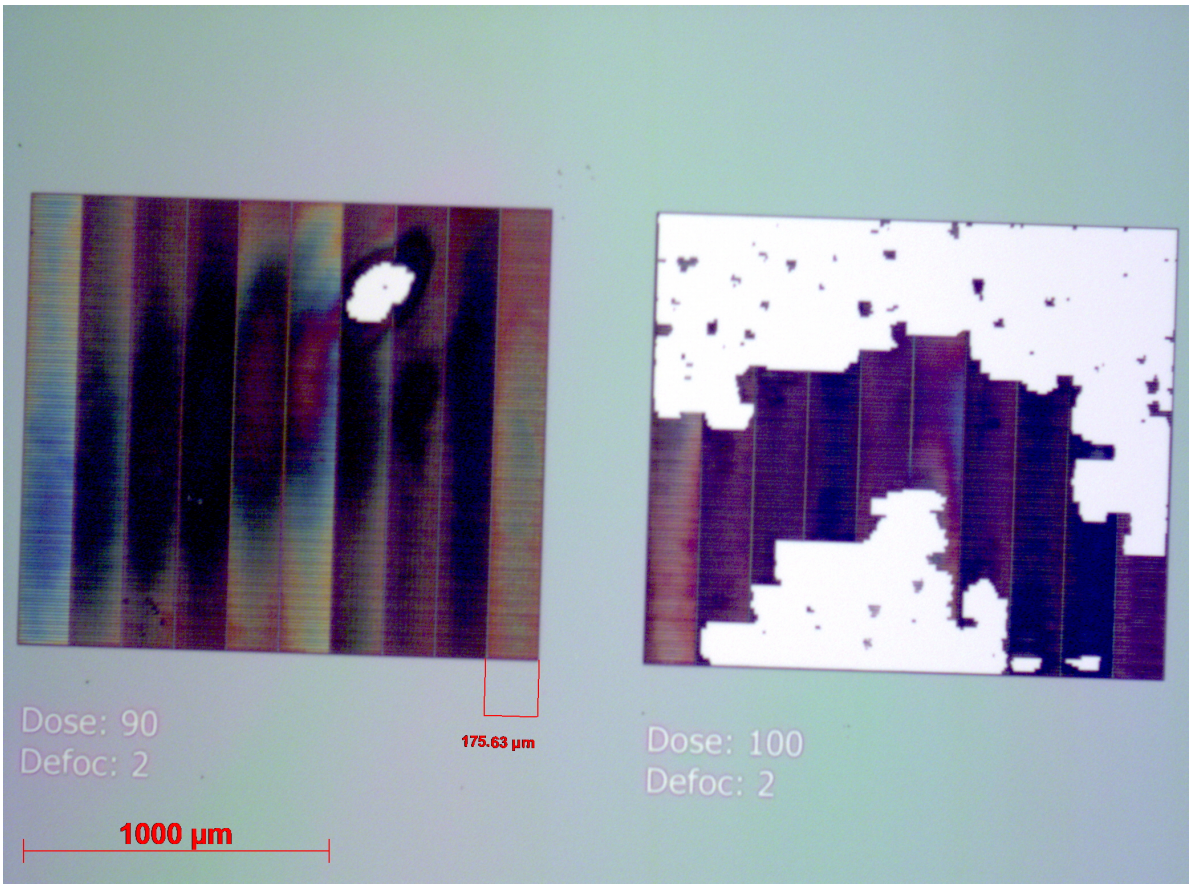

Figure 15: Microscope image from a sample where exposure dose and focus on the Maskless Aligner were varied. Doses are given in mJ/cm^2. The write field can be seen as the rectangles on the left, which indicate some damage at the edges of the write field. Ideally, no rectangles or change in color would be visible, as the exposed surface is supposed to be uniform. The adhesion problems with the photoresist can be seen on the right, where most of the photoresist has been lost during development.

Other challenges from recreating the pattern included the effects which appeared at the edge of the write field, the differing thickness of the photoresist across the sample, and particles

contaminating the surface of the sample. The write fields of the Maskless Aligner can be seen as the rectangles in the left area of Figure 15. The write field edge effects can be seen as the different colors at the edge of the rectangles, while the changes in thickness of the photoresist can be seen as the different colors within a single rectangle. A higher magnification image of the two exposed areas can be seen in Figure 16. The difference between the exposure dose for the two areas is 10 mJ/cm^2, which has a clear effect on the result. The write field edge effects can be seen in Figure 16 (a), where the white stripe is the edge. It seems likely that the pattern has had a higher exposure at the edges, resulting in removal of more photoresist during development. These edge effects could be a result of the edges being exposed twice, which seems likely considering the alignment accuracy as given by the producer of the instrument is only "less than 500 nm"[21], which equals the radius of the exposed holes in the pattern.

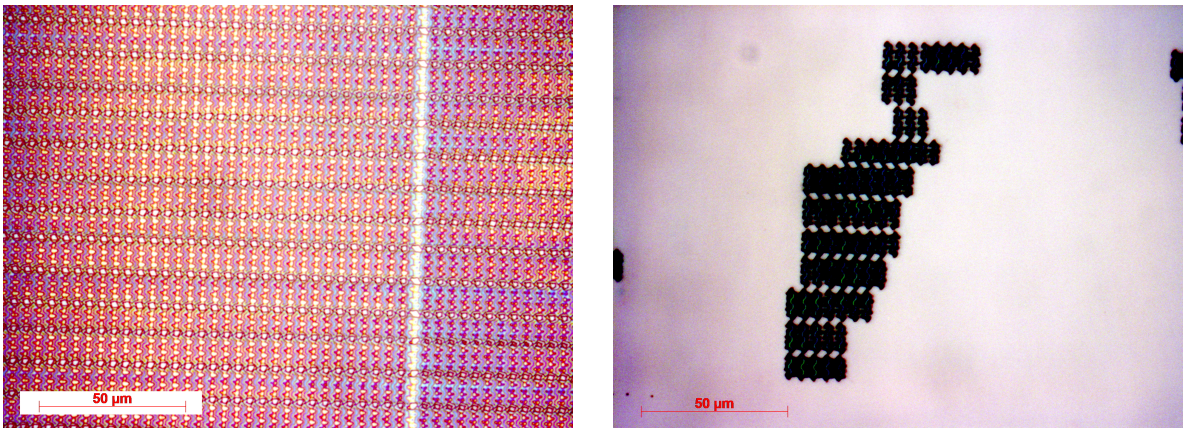

(a) (b)

Figure 16: High magnification microscope images of the exposed areas shown in Figure 15. (a) Shows the left area, which was exposed with 90 mJ/cm^2, where an edge effect can be seen as a white stripe through the pattern. For comparison, a similar high magnification image from a sample with more space between the structures, which looked good during inspection, can be seen in Figure 17. (b) Shows the right area, which was exposed with 100 mJ/cm^2, where too much of the photoresist was accidentally removed during development.

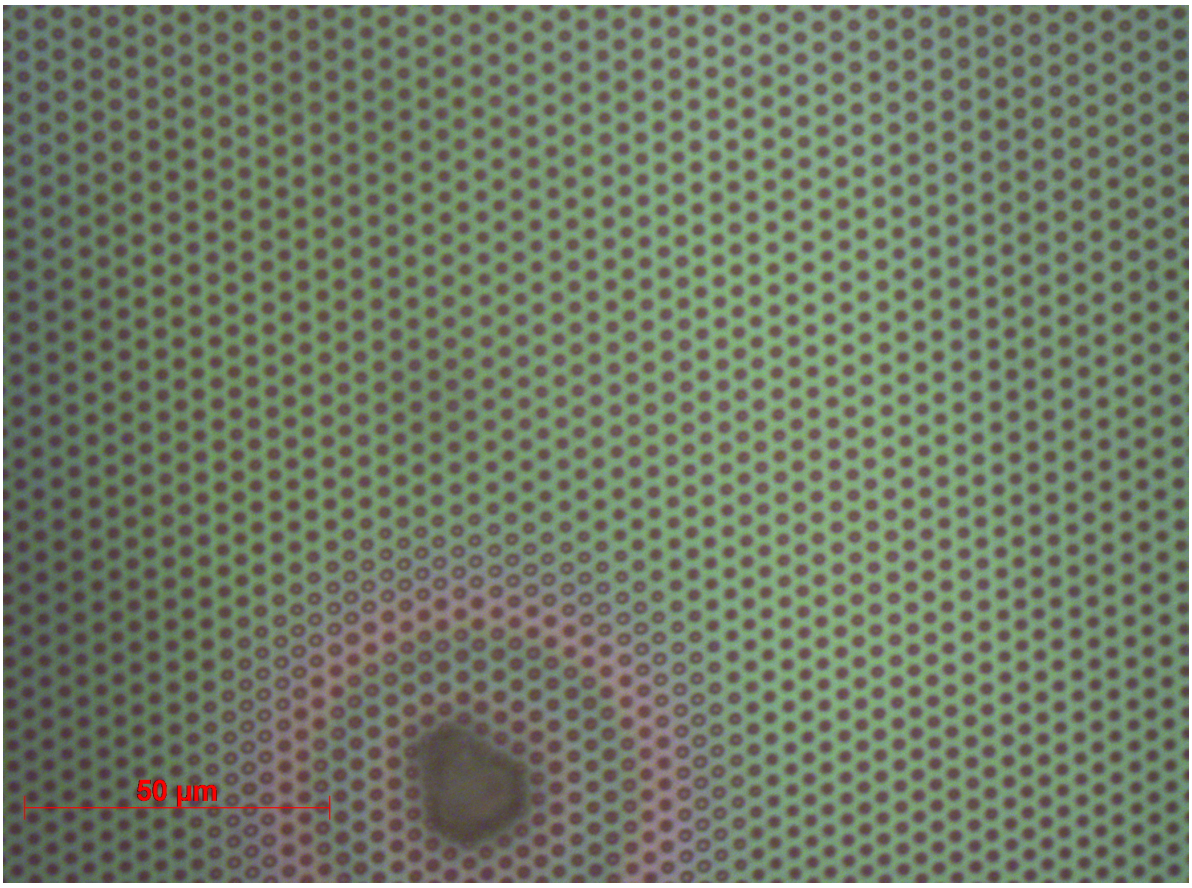

Figure 17: Microscope image from a sample where the photoresist seemed to have been developed correctly overall, but where the surface was only partially structured after etching. Damage from a particle can be seen in the image, to illustrate the form of contamination that occurred most frequently. No writefield edge effects can be seen at the surface, which was normal for correctly developed samples.

Another challenge faced when recreating the structure was that the etching step did not always etch the surface correctly. This problem mostly occurred for samples where the size of the holes was meant to be about 1 µm, according to the mask used. This issue could result in samples being partially textured, but it mostly resulted in several samples that underwent the same processing steps ending up with very different surface structures. A sample that ended up with a partially textured surface is shown in Figure 18, which shows two AFM images taken from different parts of the same surface. The result of several almost equally treated samples ending up with different surface textures can be seen from the reflection results in Figure 23, where four of the samples simply did not get etched successfully.

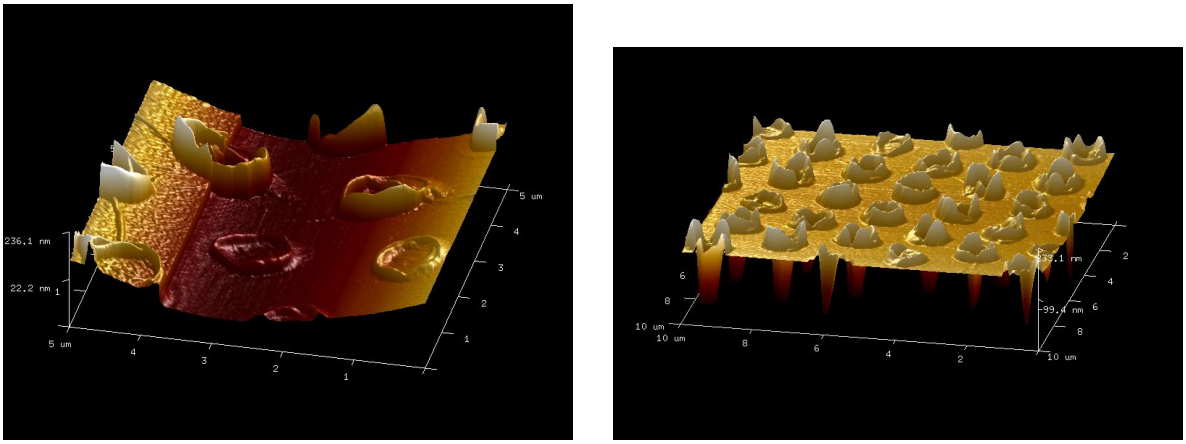

(a) (b)

Figure 18: Two AFM images taken at different areas on the same sample. (a) Shows a surface where etching has not been successfull, as can be seen by the lack of depth inside the circles. (b) Shows a surface where etching was successful, and relatively uniform.

The reasons behind the etching problems were not identified, but could be connected to the minimum feature size of the Maskless Aligner used in the exposure. The minimum feature size advertized by the producer of the instrument is at 1 µm, and for the samples where the etching problems occurred, the feature sizes were typically around 1 µm for the holes, and the same or smaller for the distances between the holes. This distances measured with AFM for one partially unsuccessful sample can be seen in Figure 19, and for that sample the hole size and distance between holes were both approximately 1 µm. Another possibility is that the small feature sizes made the whole exposure and development process very dependent on the depth of the photoresist layer, which will typically vary somewhat throughout a sample, especially if the surface is contaminated by particles. An argument speaking for this is the fact that several samples were only partially etched. There must have been some internal differences for those samples, instead of differences between the procedures followed for different samples.

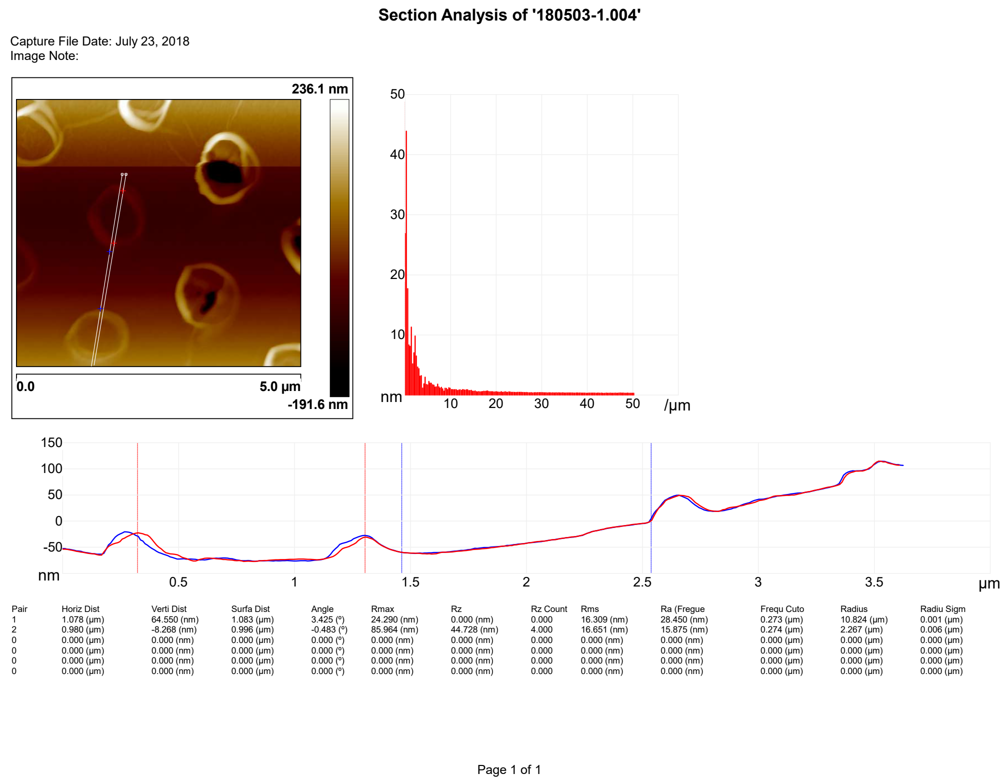

Figure 19: Distance measurements in the AFM image of the surface seen in Figure 18 (a). The blue markers are pair 1, and the red markers are pair 2.

4.1.1 Minimum feature size

In lithography, the minimum feature size of a structure is defined as the shortest distance between two features in the structure. In the honeycomb surface structure investigated in this project, the relevant distances are the size of the holes, and the distance between them. The minimum feature size that can be produced by the Maskless Aligner is 1 µm, according to the producer of the instrument[21]. The smallest features produced using the Maskless Aligner in this project is shown in Figure 20, which shows an SEM image of the sample with the closest packed holes successfully made. The smallest feature size in the figure is the distance between the holes, which was meant to be about 300 nm, is a bit difficult to determine, but at least smaller than the 1 µm advertized by the producer, but there are clearly issues with creating holes this closely packed. The height of the walls of the holes are varying greatly and periodically, which could almost be attributed to design if it wasn't for the fact that the mask used only contained a uniform hexagonal pattern of 1 µm diameter holes with 300 nm distance between them. Comparing this closely packed structure to the structure found in Figure 21, where the mask had 1.5 µm diameter holes with 700 nm distance between them, one can see that the uniformity is much better for a minimum feature size closer to the 1 µm advertized by the producer.

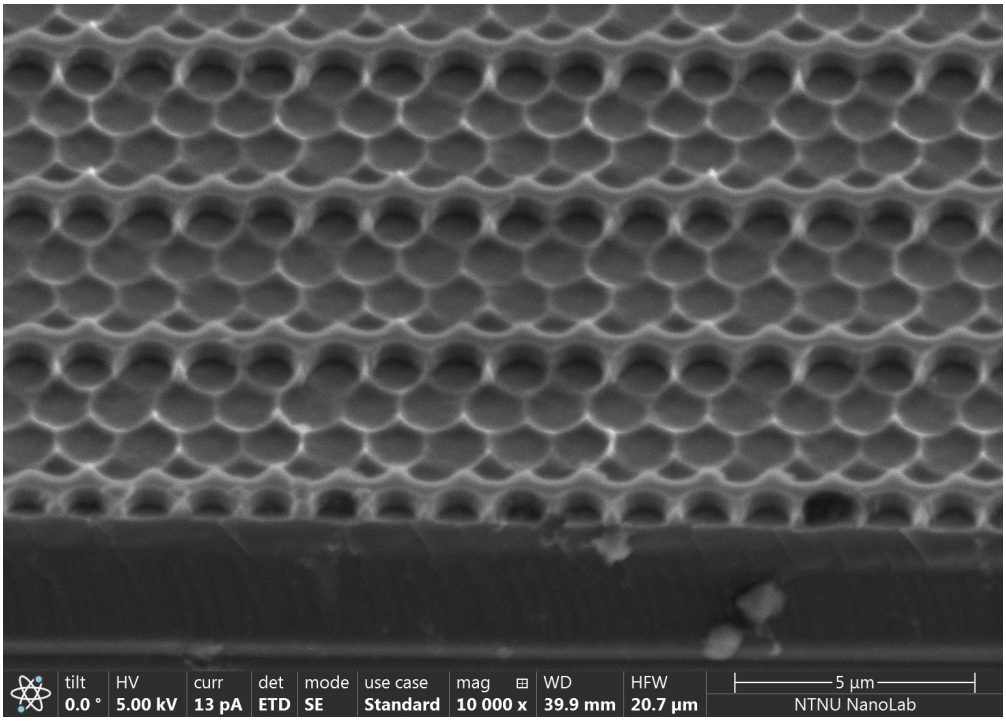

Figure 20: SEM image of a sample with a honeycomb structure where the minimum feature size was designed to be 300 nm, which resulted in a non-uniform structure with wall heights varying periodically.

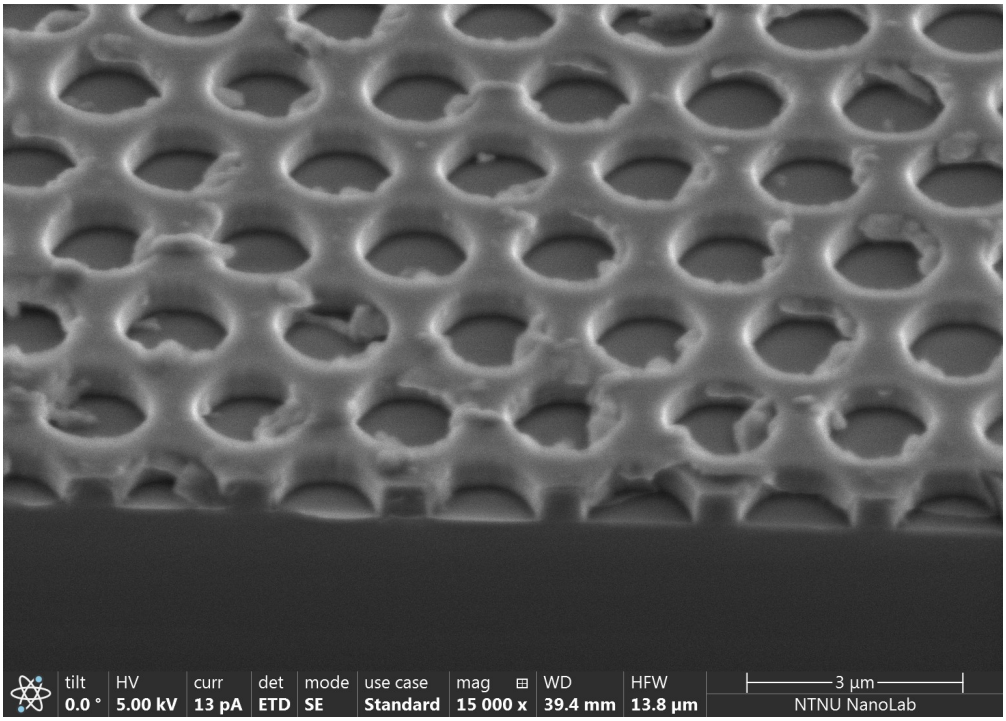

Figure 21: SEM image of a sample with a honeycomb structure where the minimum feature size was 700 nm, which resulted in a uniform structure.

4.1.2 Pattern Discussion

In general, the pattern recreation using the MLA 150 can be considered partially successful. While the feature sizes for the uniform diffractive honeycomb structures made, an example is shown in Figure 21, were not as small as the ones made using the micro-lens array, an example is shown in Figure 5, they were still small enough to cover significant parts of the surface. And less uniform structures were made which quite closely resembled that of the micro-lens array structures, as can be seen in Figure 20.

Some issues were discovered during the experiments, which did affect the structures created significantly, most prominent among them were the loss of adhesion for unexposed photoresist during development, and the somewhat unreliable etching process. The adhesion issues might be traceable back to the reduced cleaning procedures discussed in Section 3.1.2, but could also be connected to the photoresist layer thickness. It was decided early on, after discussions with the NanoLab staff, to use a photoresist thickness of about 1 µm, but this might not have been the optimal photoresist thickness. Thicker photoresist layers might have been more rigid, and therefore stuck onto the surface of the wafer better, but on the other hand, they might have reduced the effective feature size of the Maskless Aligner because the exposing light would have had to pass through a thicker layer, which might defocus and scatter the light somewhat. This in turn could have contributed to making the etching

process even more unreliable, if those problems were indeed connected to the smallest feature size restrictions of the Maskless Aligner.

4.2 Reflection measurements

The second goal of the thesis was to investigate the hole depth, hole width and coverage ratio using reflection measurements. The reflection measurement results are split into three sections. As it can be somewhat difficult to compare the samples using reflection curves alone, average values from the different series are also presented and compared. In order to lower the standard deviation values for the averages, reflection values for wavelengths under 400 nm were excluded from the average, as those tend to deviate largely from the average.

As described in Section 4.1, some samples did not get etched correctly, even though the process steps followed did not differ from other samples in the same series. The difference in surface texture etched as illustrated in Figure 18, however, indicates the presence of some degree of surface structure. The reflection values of some of these unsuccessful structures were also measured, and an example can be seen in Figure 22. It is clear from the figure that the unsuccessful structures did not contribute meaningfully to the light trapping performance, as they have the same reflection values as a polished sample.

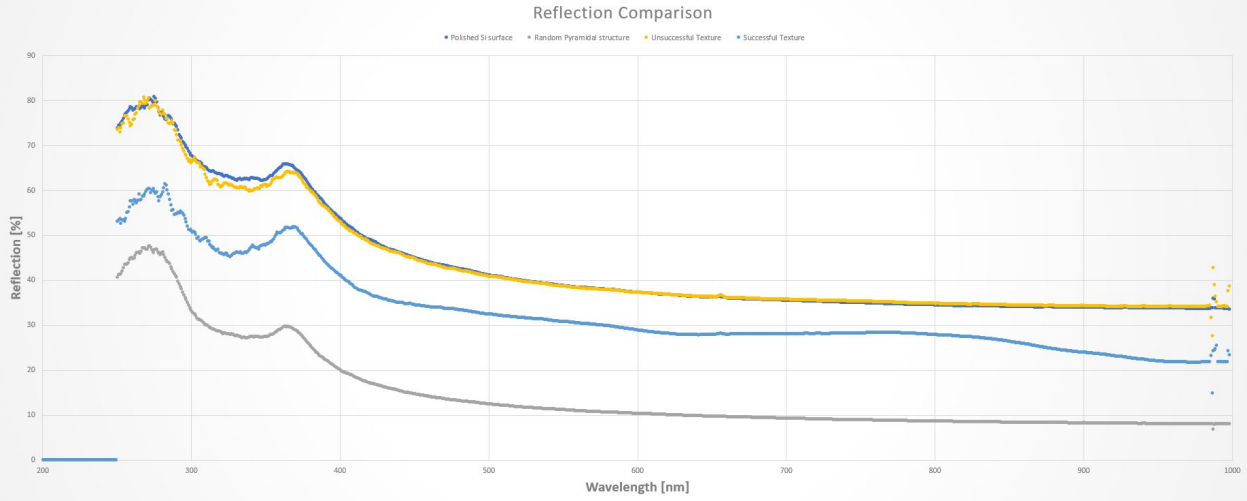

Figure 22: The reflection values measured to compare an unsuccessful structure (sample 1 from depth variation) to a polished wafer, a successful structure, and a pyramidal structure.

4.2.1 Depth variation results

The reflection curves from the depth variation experiment can be seen in Figure 23. Most of the samples for the depth experiment did not result in usable reflection measurements, as can be seen by the similarity in most of the reflection curves from sample 1 through 4. As

the reflection for sample 1 is also shown in the comparison in Figure 22, and sample 2,3 and 4 have similar values, it seems likely that the surface structure was not correctly etched into the samples.

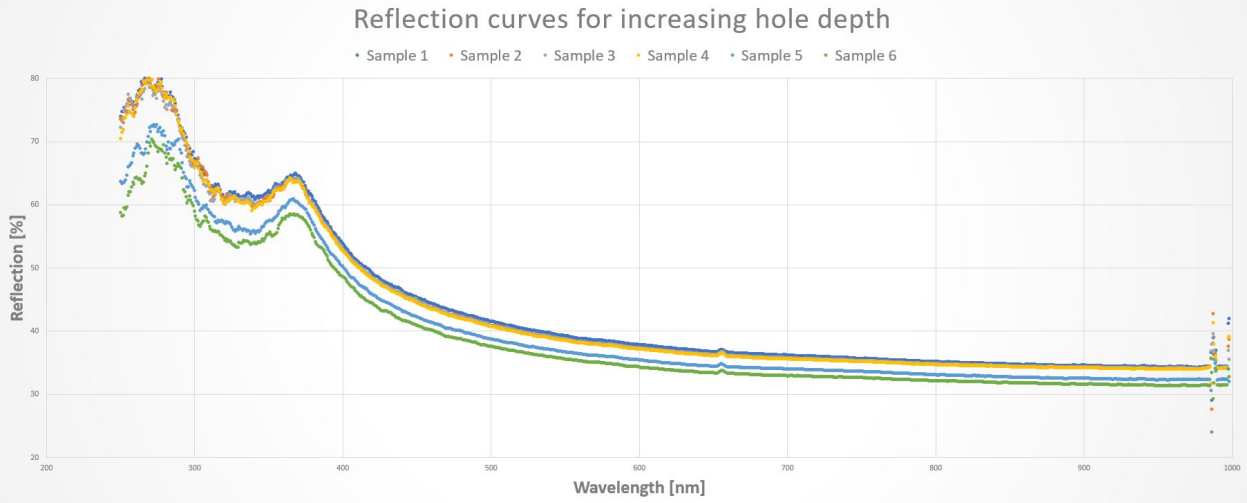

Figure 23: The reflection values measured for samples where the depth of the holes in the honeycomb structure varied. The depth was designed to be at 150, 300, 450, 600, 750 and 900 nm for sample 1 to sample 6 respectively, but the structures were not successfully made for most of the samples.

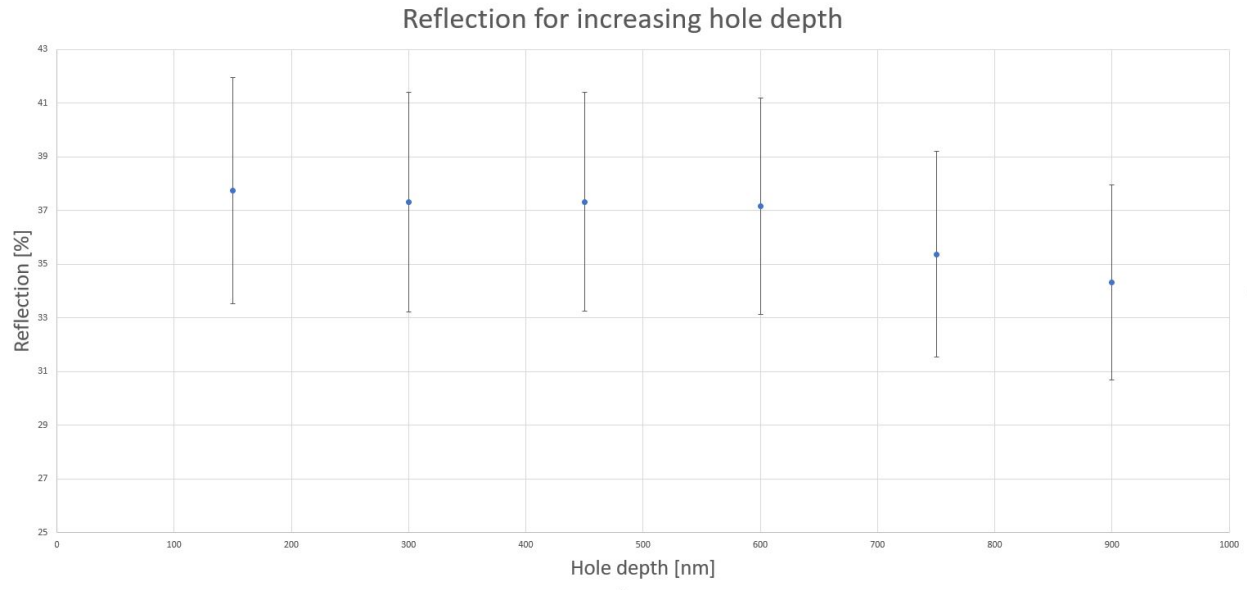

Figure 24: The mean reflection values from 400 nm and up, measured for samples where the depth of the holes in the honeycomb structure varied. The samples are the same as shown in Figure 23.

4.2.2 Hole width variation results

The reflection curves from the samples where the hole width was varied, meaning the ratio between the width of the holes and the depth of the holes, are displayed in Figure 25. In these samples, the width of the holes was approximaetly 1, 1.5, 2, 2.5, 3, 3.5, 4 and 4.5 µm for sample 1 through 8 respectively, while the depth remained the same, at approximately 500 nm. The results are somewhat difficult to determine, since there is very little difference between the curves. An average of the reflection values from 400 nm and up can be seen in Figure 26, but as the size of the error bars suggests, these are not any clearer to determine the most effective hole width. It was expected that sample 1 would have the lowest reflection of all these samples, and thus the best hole width, based on findings in Thorstensen's Ph.D[1].

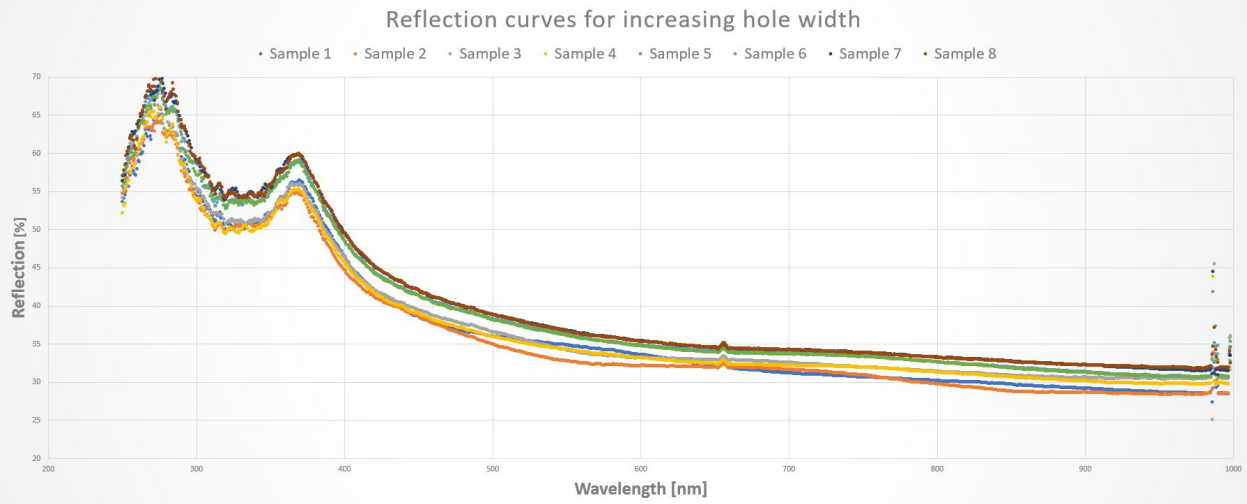

Figure 25: The reflection values measured for samples where the hole width of the holes in the honeycomb structure varied. The width was increased from about 1 µm for Sample 1, to about 4.5 µm for Sample 8.

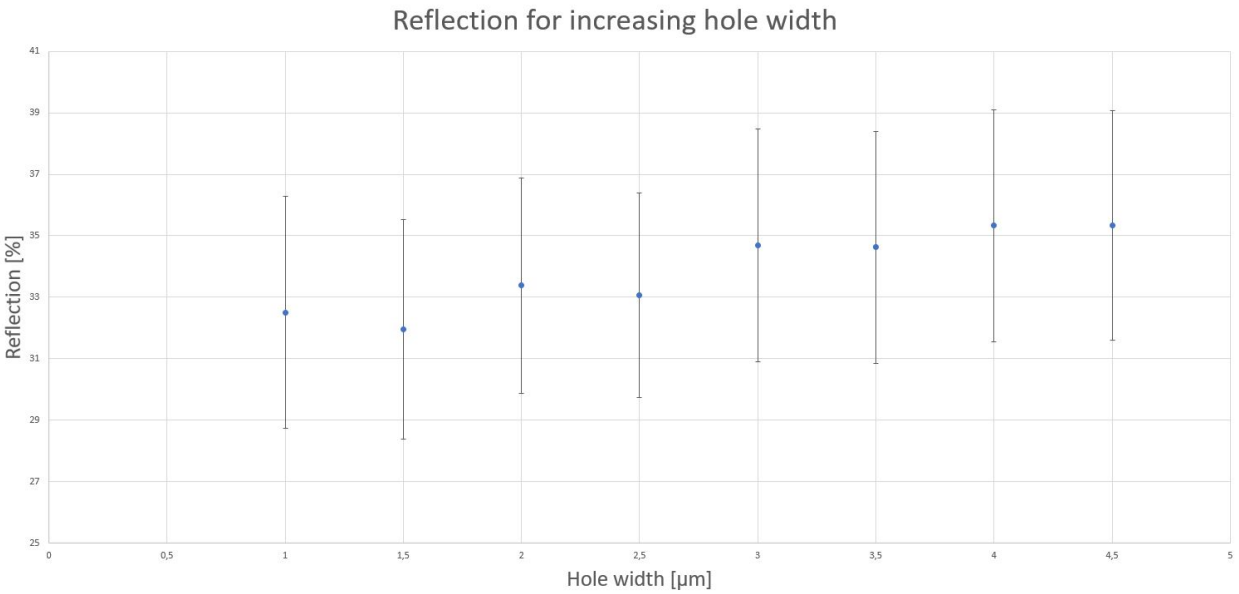

Figure 26: The mean reflection values measured from 400 nm and up, for samples where the hole width of the holes in the honeycomb structure varied. The samples are the same as shown in Figure 25.

4.2.3 Coverage ratio variation results

The coverage ratio is in this context defined as the ratio of hole area to total area on the surface of the sample, meaning that the smaller the distance between the holes, the larger the coverage ratio, when the hole sizes stay the same. Here, the hole sizes remained static at 1 µm, while the distances between the holes were increased linearly from 300 nm in sample 1 to 1700 nm in sample 8. The reflection curves from the samples where the coverage ratio was varied are displayed in Figure 27. These reflection curves show the largest differences between the samples, out of all the reflection results. And interestingly enough, samples 1, 3, and 4 show the lowest reflection, while the rest are somewhat higher and sample 8 is quite a lot above the rest. These results fit quite nicely with the average values from 400 nm and up as shown in Figure 28. However, also here the error bars are quite large, probably due to the fact that a normal average might not the most efficient way of compressing the measurement results into one number.

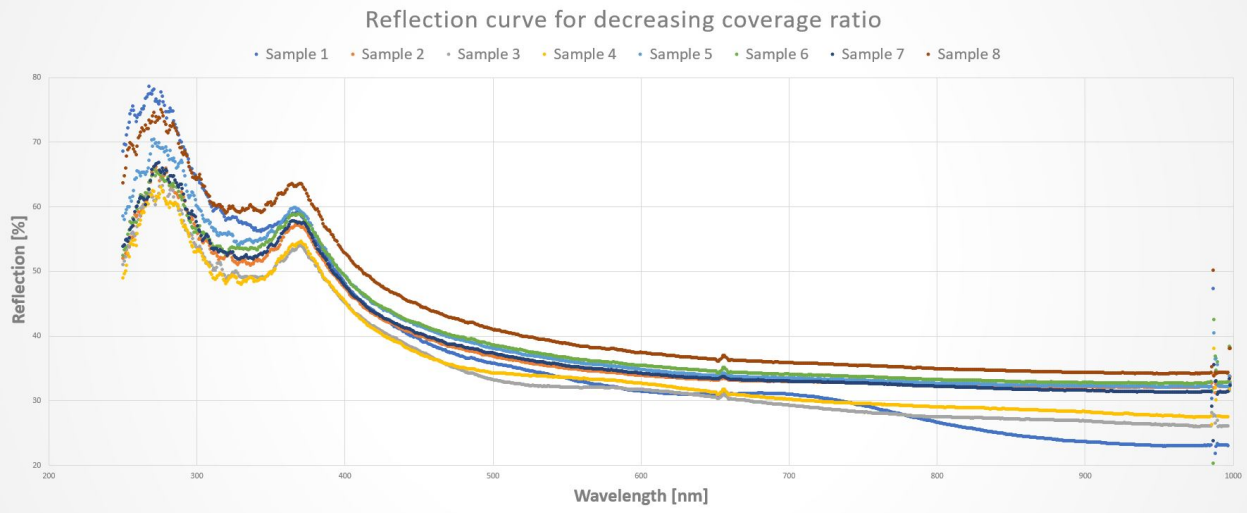

Figure 27: The reflection values measured for samples where the coverage rate of the honeycomb structure varied. The hole size was kept static at about 1 µm, while the distance between the holes were 300, 500, 700, 900, 1100, 1300, 1500, 1700 nm for sample 1 to sample 8 respectively.

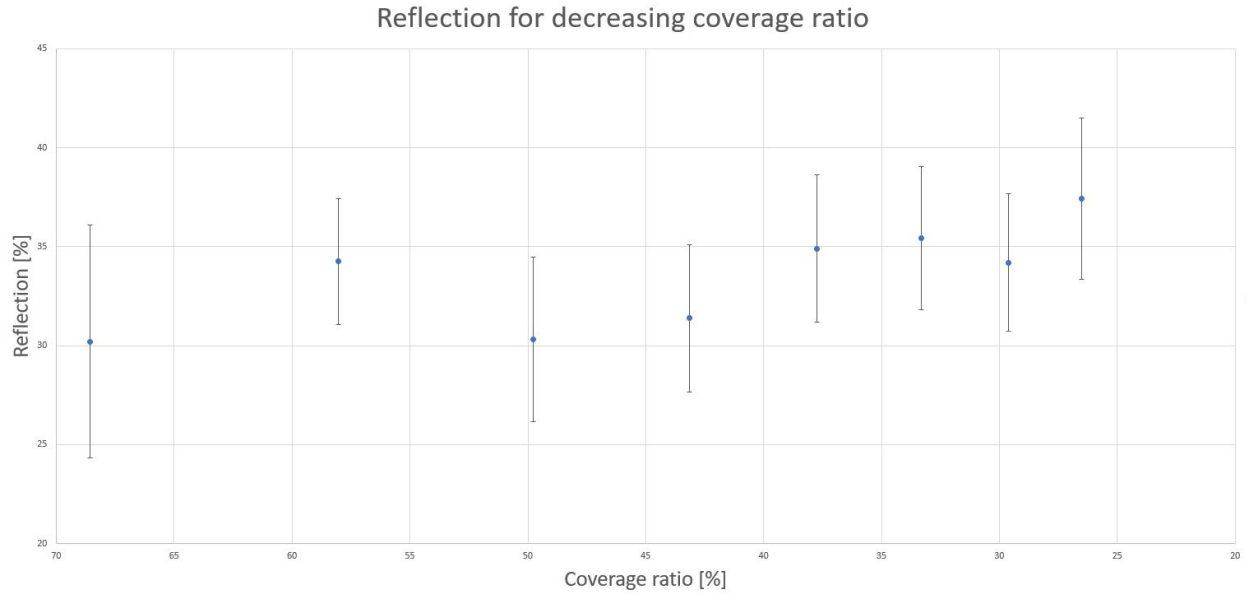

Figure 28: The average reflection values measured from 400 nm and up, for samples where the coverage rate of the honeycomb structure varied. The samples are the same as shown in Figure 27.

4.2.4 Reflection results discussion

The results from the reflection measurements do not clearly point towards a specific combination of parameters which would make the ideal diffractive honeycomb structure. However, there are a few trends that might be extracted from the measurements. From Figure 26, one could say that the reflection begins low with sample 1 and 2, and increases towards the later samples. From the reflection curves shown in Figure 25, there seems to be a divide between sample 1-4 and sample 5-8, indicating that a hole width lower than or equal to about 2.5 µm has lower reflection than for larger widths.

The measurements from the depth variation shown in Figure 23 indicate that several of the samples were not etched correctly, it is therefor difficult to extract information on any trend for those samples. For sample 5 and 6, with depths at about 750 nm and 900 nm, the results indicate that deeper holes have lower reflection values, but considering the few samples available, this is somewhat unreliable. Since the reason for the unreliable etching was not identified, the most certain way to get better results would have been to etch enough samples so that at least one full successful series could have been studied. Alternatively, assuming that the feature size is the issue, the series could have been made with significantly larger hole diameter, at for example 2 µm, as these were more reliably etched. This was not considered when the depth variation samples were made, as it was believed the change might have altered the diffractive structure significantly. When considering the results from the hole width variation shown in Figure 25, it seems clear that holes wider than 1 µm also creates a low reflection structure, and thus could have been used for the depth variation.

When looking at the results from the coverage ratio measurements shown in Figure 27, and the average values presented in Figure 28, there is a trend towards the first samples having lower reflection values, which fits with expectations that higher coverage leads to lower reflections. This trend is not as clear as was expected, however, considering sample 2 is sort of an outlier. An interesting result from the coverage test is the dip at the end of the curve for sample 1. This looks like it could be due to an unintended diffractive effect, since in this wavelength range the curves are usually relatively flat, as indicated by the other curves in the same figure, but also seen in the pyramidal texture shown in Figure 22. The sudden dip could be due to a periodicity in the structure which the other structures lack, or it could be due to the smaller distance between the holes, as sample 1 has the smallest distance between the holes at a designed distance of 300 nm. An argument for this effect being the result of a separate periodicity in sample 1, can be made on the basis of Figure 20, which shows the surface of this sample. In the figure, a clear periodicity can be seen parallell in direction with the edge, which is not meant as an actual part of the structure, but has occurred based on some other factors. A factor could be limitations in the minimum feature size of the Maskless Aligner, as discussed in Section 4.1.1, perhaps due to interference or the way the write field is calculated and converted.

4.3 Lifetime measurements

The last overall goal of the thesis was to investigate how the surface structures effect the minority carrier lifetime in the wafers. The results from the lifetime measurements can be seen in Figure 29, and the results from the reference that was not etched can be seen in Figure 30. While it may seem that the measurements were performed differently, since the graphs are of very different lengths at the x-axis, this was not the case. Since the QSSPC method measures lifetime as a function of excess minority carrier concentration, also called injection level, it can only measure the lifetime up to the maximum excess carrier concentration achieved during the illumination, and that maximum concentration varied greatly for the different samples.

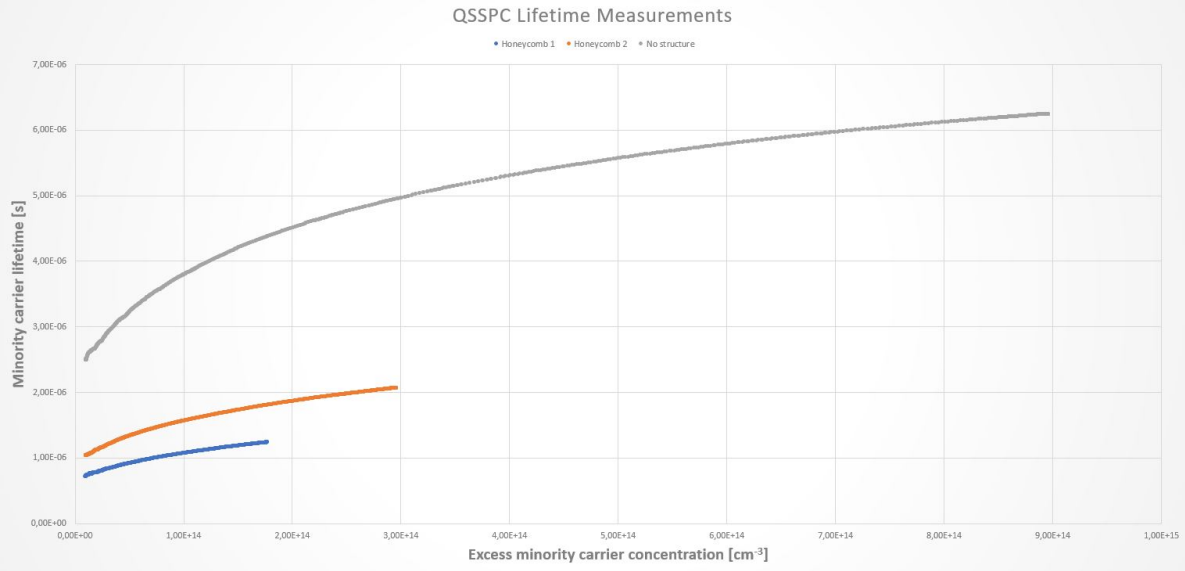

Figure 29: The graphs show the minority carrier lifetime as a function of injection level, for three different samples. All three samples were etched using ICP-RIE. The "Honeycomb 1" sample has a high-coverage structure, where the distance between the holes was made as short as possible, with a goal of 700 nm distance. The "Honeycomb 2" sample has a lower coverage structure, where the distance between the holes was made significantly larger, with a goal of 1.5 µm distance. The "No structure" sample did not have any photoresist layer, but was still etched with the other two, in order to see how the structure affects the lifetime.

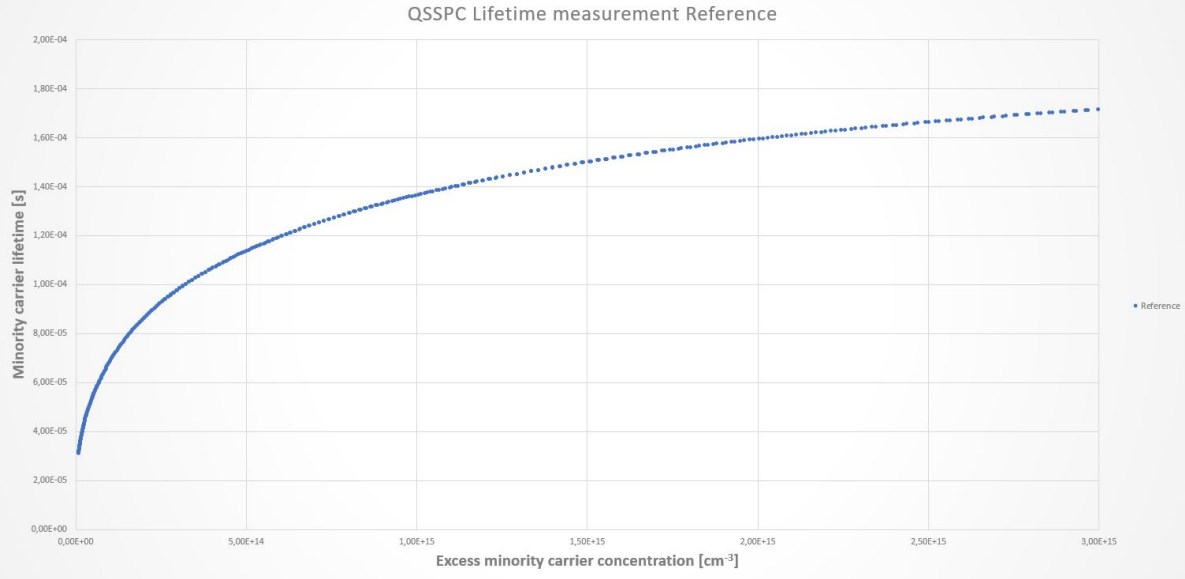

Figure 30: The graph shows the minority carrier lifetime as a function of injection level for a reference sample that was not etched in the ICP-RIE, but was passivated along with the other samples using PECVD. As can be seen, the lifetime measured was much greater than in Figure 29, which was expected, but it was only at about a tenth of the lifetimes normally measured for that kind of wafers.

When comparing the lifetime of all the samples at an injection level of 10^{14} cm^{-3} (1,00E+14), as listed in Table 1, it is clear that the ICP-RIE method of etching has an adverse effect on the minority carrier lifetime of the samples. This is clear when comparing the three samples that were etched to the "Reference" that was not, and was also expected. The most surprising result was the reference sample, which was expected to have a minority carrier lifetime well above 1 ms at an injection level of 10^{15} cm^{-3}, but the values measured were only in the range of a few µs, as can be seen in Figure 30. This indicates that either the passivation process also affected the lifetime negatively, since that is the only process which the reference was put through, or that the batch of wafers were of a much lower quality than normal, which seems very unlikely considering that the producer of the wafer, Topsil, guarantees a certain lifetime for all the wafers they sell, and no abnormalities were reported in the other wafers from the same batch. Therefore, it seems very likely that the passivation process is the culprit, and as described in Section 3.8.1, that the maintenance work prior could have affected the passivation process, because a proper clean program was not run at the start of the passivation process.

Table 1: Comparison of lifetime values at a certain injection level. Lifetime curves for the samples are shown in Figure 29 and Figure 30.

Sample	Lifetime at injection level 1E+14 [µs]
Reference	68
No structure	3.8
Honeycomb 2	1.5
Honeycomb 1	1.1

Since the minority carrier lifetimes measured were a lot lower than expected, it was of interest to consider the PL images from the samples, which represent the photogeneration rate in the samples during the steady state illumination. These can be seen in Figure 31.

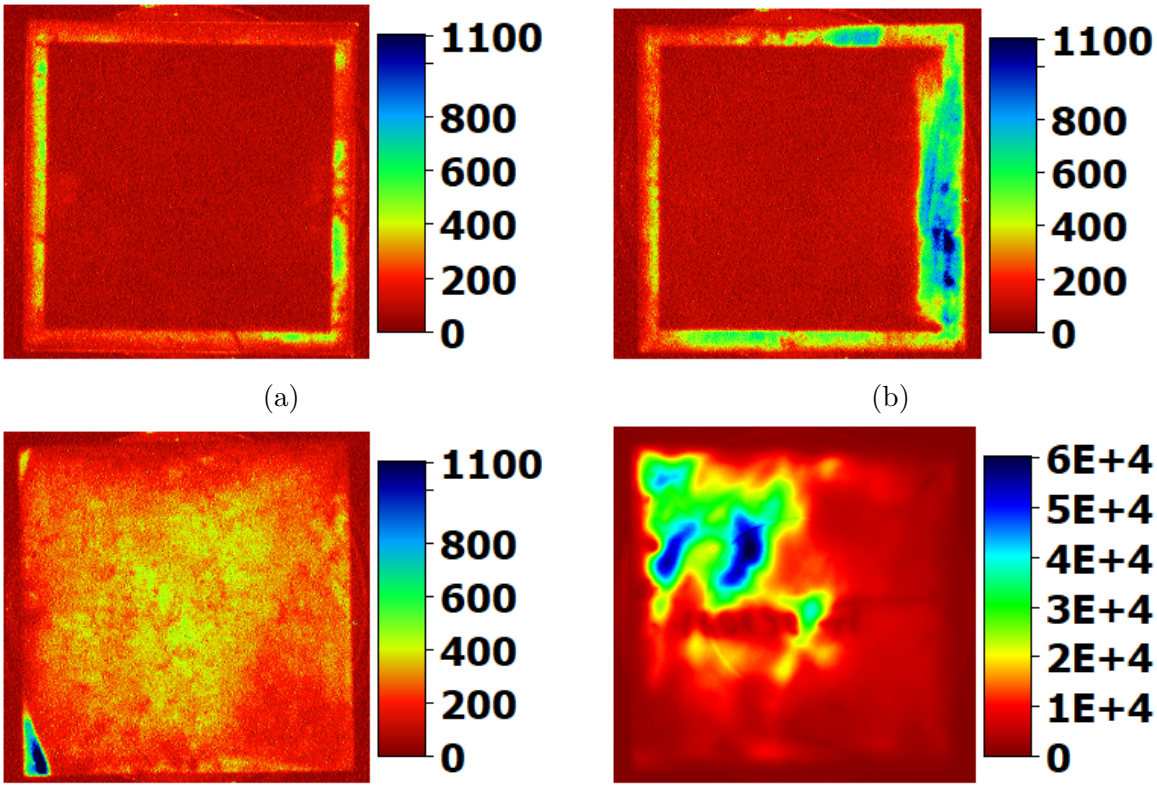

Figure 31: The images show uncalibrated PL images where the colors represent photon-generation by counts. (a) Shows a high coverage honeycomb structure, (b) shows a low coverage honeycomb structure, (c) shows a sample which has been etched in the ICP-RIE process without photoresist, and (d) shows a reference samples which was not etched. The square frames which can be seen in (a) and (b) are the un-textured edges of the sample. The large difference in counts between (d) and the rest illustrates how low the counts were for the etched samples. Important to note here, is the counts seen outside of the sample edges, which represent the background noise. This noise is very relevant for (a) and (b), where the inside of the frame is almost indistinguishable from the outside noise, while this is not the case for (c) and (d).

4.4 Lifetime discussion

Assuming that the lifetime measurement results were somewhat reliable even with the unsuccessful passivation, it seems likely that the diffractive honeycomb structure does somewhat lower the lifetime of the minority carriers, as can be seen in Table 1. It is quite clear that the ICP-RIE etching affects the lifetime negatively, as the reference sample has a much higher lifetime than the others. It also looks like a higher coverage of the surface leads to lower lifetimes as well, which might be related to the fact that a low coverage structure will have

less of the surface exposed to the ICP-RIE etching process. From the Figure 21 and 10, one can see that the diffractive honeycomb structure surfaces tend to have artifacts of different kinds, which might function as recombination centers, further supporting the theory that a higher coverage pattern will have a lower minority carrier lifetime. This fits with a general understanding of recombination at surfaces, where defects and damages contribute to recombination by acting as recombination centers[9].

On the other hand, it is also possible that the lifetimes measured are so low that the measurements are not reliable enough for comparing the diffractive honeycomb structures effect on the minority carrier lifetime. When looking at Figure 31 (a) and (b), it is difficult to argue that the counts coming from inside the sample frames are significantly higher than the noise seen outside the sample frames. Thus, the very low values of the minority carrier lifetime measured for the two honeycomb structures, might have been affected significantly by noise, or by the frames of the sample. Additionally, the right edge which can be seen in (b) was damaged during the experimental process, and not etched correctly. Since the counts coming from this edge are clearly higher than the rest of the sample, this damage might have contributed significantly to the higher lifetime measured in the low coverage honeycomb structure, since a large part of the structures were simply not made. Therefore, it seems likely that the lifetime measurement results are not reliable enough for comparison of coverage ratio for the honeycomb structure. However, it seems likely that the results can be used for comparing between structured and unstructured samples, since Figure 31 (c) shows a decent count difference between inside the frames and outside, indicating that the counts inside are significantly higher than the background noise.

5 Conclusion

In this thesis work, the diffractive honeycomb structure for silicon wafers developed by Thorstensen[1], was recreated with partial success, using photolithography, the Maskless Aligner 150, and an ICP-RIE etching method. The finished structures were investigated using SEM and AFM techniques. Some issues were faced when trying to minimize the distance between the holes, such as the minimum feature size of the Maskless Aligner, and adhesion problems for the photoresist during development. While the feature size issue might be difficult to improve upon while still using the Maskless Aligner, utilizing other lithography techniques might solve this issue. For the adhesion issues, utilizing a more comprehensive cleaning procedure might solve the issue, but using thicker photoresist layers could also potentially work. Another issue faced was connected to uneven etching, which resulted in several samples ending up only partially textured, or not textured at all. This issue was not solved, but could be connected to the minimum feature size of the Maskless Aligner.

Furthermore, three important parameters of the diffractive honeycomb structure were varied, and their effect on the reflection was investigated. The hole depth was investigated by trying to create samples with 1 µm diameter holes and depth ranging from 150 nm to 900 nm, and then measuring the reflection from the samples. However, several of the samples were not etched correctly, and ended up without any significant surface structures. This made the reflection results from this series unreliable, and while the results indicated 900 nm depth had lower reflection than 750 nm depth, no trends could be extracted from the 150 - 500 nm range.

Another parameter investigated was the width of the holes, which was done by keeping the hole depth static while varying the hole width for the samples. The hole depth was kept at about 500 nm, while the width was varied from 1 µm to 4.5 µm. The results from these measurements indicated that a hole width lower than or equal to about 2.5 µm has lower reflection than for larger widths. However, a single optimal hole width was not clearly identified.

The last parameter investigated was the coverage ratio of holes to surface area, which was done by keeping the hole depth and width static, while varying the distance between the holes. The hole depth was kept at about 500 nm, the hole width at about 1 µm, and the distance was varied from about 300 nm to about 1700 nm. In these results, there was an overall trend towards lower distances, meaning higher coverage, resulting in lower reflection values, where samples with distances below 900 nm generally had lower reflections, but the individual measurements still varied somewhat. An interesting effect occured for the smallest sample with 300 nm distances, which showed a dip in the reflection curve in an unusual range of wavelengths, indicating some sort of unintended diffraction effect. This might have been the result of an unintended periodicity in that sample, which occured for reasons which were not identified, but possibly connected to the minimum feature size for the Maskless Aligner used for producing the samples.

The last overall goal of the thesis was to investigate the impact of the diffractive honeycomb pattern on the minority carrier lifetime in the wafer. This was done with floatzone wafers, because of their good electrical properties. Four samples were made, two with different structures, one without a structure but still etched with the others, and one that was not etched, for reference. All four were passivated using PECVD to deposit amorhphous silicon, then the lifetime was measured using the QSSPC method. The results of the lifetime measurements were much lower than expected for all samples, including the reference. Since nothing abnormal about the wafer batch had been noticed in other situations, it seems likely that the lack of a proper clean of the reaction chamber in the PECVD system before the passivation process was to blame. Due to the poor lifetime measurement results, it was difficult to point out a clear trend in the results, but they indicated that the diffractive honeycomb pattern does lower the minority carrier lifetime.

6 Future Work

As several of the investigations done in this thesis work did not identify optimal parameters, there are possibilities of continued work on this topic in the future. Some parameters that could be changed for potentially better results are listed below:

1. The cleaning process. This can be made more thorough and comprehensive, as discussed in Section 3.1.2, which might lead to less issues with the photoresist.
2. Photoresist thickness. The photoresist thickness used in the experiments was about 1 µm, and a thicker resist layer might have resulted in more rigid structures with better adhesion, and thus prevented some of the problems faced during delevopment. On the other hand, a thinner resist might have improved the reliability of the etching step. This is discussed in Section 4.1.
3. Depth variation: The width of the holes used in the depth variation, which was 1 µm, could have been wider, as samples with hole width at for example 2 µm were more reliably etched. This could have reduced the reliability problems with the etching, and thus improved the results from the reflection measurements.
4. Aspect and coverage ratio: More samples at lower aspect ratios and higher coverage ratios might result in clearer trends and improving the chances of identifying optimal parameters.
5. Passivation for lifetime: Simply redoing these samples, while making sure the PECVD reaction chamber is clean before passivation, could lead to more reliable results. Additionally, calculating the surface recombination velocity could be done if the bulk minority carrier lifetime of the wafer is known.

An alternative to altering the specific parameters used in this thesis, however, is to create the diffractive honeycomb structures using other methods than photolithography and a maskless aligner, as these probably contributed to several of the issues faced in the work. EBL might be a feasible method, if a solution is found for producing structures with several millions of objects, or alternatively using a reflection instrument with a much smaller focus spot so that structures can cover a smaller area than the ones used in this project, and thus fewer holes would be needed.

A perhaps more important avenue for further work, is in trying to adapt the diffractive honeycomb structure to industry. This involves finding a way to process a wafer surface in a sufficiently short amount of time, with reasonably cheap means, and a decent resulting structure. The most promising way to do this still seems to be using a pico second pulse laser, with either a monolayer of self-organizing beads, or a mask like the micro-lens array. This texture seems to have potential in industry based on the novel wafer production methods being investigated, with both diamond wire sawing of multi-crystalline wafers, and kerfless production of wafers with surface crystal orientations different than <100>.

Abbreviations

Table 2: Overview of abbreviations used in the thesis.

Abbreviation	Explanation
As	Element: Arsenic
AFM	Atomic force microscopy
CCD	Charge-coupled device
DI	De-ionized
EBL	Electron beam lithography
F	Element: Fluor
Ga	Element: Gallium
GB	Gigabyte
H	Element: Hydrogen
ICP	Inductively coupled plasma
ICP-RIE	ICP-Reactive ion etching
IFE	Institute for Energy Technology
K	Element: Potassium
KB	Kilobyte
MLA 150	Maskless Aligner 150
N	Element: Nitrogen
NTNU	Norwegian University of Science and Technology
O	Element: Oxygen
PECVD	Plasma enhanced chemical vapor deposition
Ph.D	Philosophiae Doctor
PL	Photoluminescence
PV	Photovoltaic
QSSPC	Quasi-steady state photo conductance
R&D	Research and development
RCA	Radio Corporation of America
RPM	Rounds per minute
SEM	Scanning electron microscope
Si	Element: Silicon

References

[1] Jostein Thorstensen. Laser processing for thin and highly efficient silicon solar cells. *Ph.D thesis*, 2013.

[2] Cheetah project. http://www.cheetah-project.eu/. Accessed: 2017-12-15.

[3] Snapshot of global pv markets 2016. http://www.iea-pvps.org/fileadmin/dam/public/report/statistics/IEA-PVPS_-_A_Snapshot_of_Global_PV_-_1992-2016__1_.pdf. Accessed: 2017-12-15.

[4] Hideyuki Asai Hidetaka Takato Isao Sakata Takayuki Aoyama, Yoichi Kondo. Fabrication of single-crystalline silicon solar cells using wafers sliced by a diamond wire saw. *5th World Conference on Photovoltaic Energy Conversion*, 2010.

[5] B. Steinhauser J. Bendick S. Lindekugel M. Hermle S. Janz S. Reber N. Milenkovic, M. Driessen. 20% efficient solar cells fabricated from epitaxially grown and freestanding n-type wafers. *Solar Energy Materials & Solar Cells*, 159:570–575, 2017.

[6] Jingjiao Zhang Xiaoya Ye Jianjiang Li Shuai Zou Xiadong Su Fang Cao, Kexun Chen. Next-generation multi-crystalline silicon solar cells: Diamond-wire sawing, nano-texture and high efficiency. *Solar Energy Materials & Solar Cells*, 141:132–138, 2015.

[7] T. Markurt D. Uebel Th. Teubner T. Boeck C. Ehlers, R. Bansen. Solution growth of si on reorganized porous si foils and on glass substrates. *Journal of Crystal Growth*, 468:268–271, 2017.

[8] E. Haugan J. Thorstensen, J. Gjessing and S. E. Foss. 2d periodic gratings by laser processing. *Energy Procedia*, 27:343–348, 2012.

[9] A.G Aberle. *Crystalline silicon solar cells: advanced surface passivation and analysis*. Sydney: University of New South Wales, Centre for Photovoltaic Engineering, 1999.

[10] B Van Zeghbroeck. Principles of semiconductor devices (2011). https://www.azonano.com/article.aspx?ArticleID=3995. Accessed: 2017-11-21.

[11] Material thickness. http://www.pveducation.org/pvcdrom/design/material-thickness. Accessed: 2017-12-15.

[12] T. Tiedje, E Yablonovich, G.D. Cody, and B.G. Brooks. Limiting efficiency of silicon solar cells. *IEEE TRANSACTIONS ON ELECTRON DEVICES*, ED-31, 1984.

[13] Erik Stensrud Marstein Sean Erik Foss Jostein Thorstensen, Jo Gjessing. Light-trapping properties of a diffractive honeycomb structure in silicon. *IEEE JOURNAL OF PHOTOVOLTAICS*, 3:709–715, 2013.

[14] E. Hasegawa M. Kawakami M. Ohwada M. Morita, T. Ohmi. Growth of native oxide on a silicon surface. *Journal of Applied Physics*, 68:1272, 1990.

[15] Charles B. Musgrave Jeung Ku Kang. The mechanism of hf/h2o chemical etching of sio2. *The Journal of Chemical Physics*, 116:275, 2002.

[16] B. E. Deal C. R. Helms. Mechanisms of the hf/h2o vapor phase etching of sio2. *Journal of Vacuum Science Technology A*, 10:806, 1992.

[17] Irving University of California. Cleaning procedures for silicon wafers. https://www.inrf.uci.edu/wordpress/wp-content/uploads/sop-wet-silicon-solvent-clean.pdf. Accessed: 2018-03-15.

[18] Chetan Singh Solanki. *Semiconductor Manufacturing Technology*. San Val, 1995.

[19] Photolithography. http://www.me.ntut.edu.tw/introduction/teacher/lu/IC%20fabrication_GA/IC_ch Accessed: 2018-07-15.

[20] Rohm and Haas Electronic Materials. Megaposit spr 700 series photoresist. *SPR-700 user guide, 2004*.

[21] Heidelberg Instruments. Maskless aligner. https://www.himt.de/index.php/MLA150.html. Accessed: 2018-07-02.

[22] A Plasma-Therm Company Corial. Inductively coupled plasma – reactive ion etching (icp-rie). https://www.corial.com/en/technologies/icp-rie-inductively-coupled-plasma-reactive-ion-etching/. Accessed: 2018-07-19.

[23] NTNU. Instruments available in ntnu nanolab's cleanroom. https://www.ntnu.edu/nano/cleanroom/equipment. Accessed: 2018-07-10.

[24] Adam De Gree. The history and working principle of the scanning electron microscope (sem). https://www.azonano.com/article.aspx?ArticleID=3995. Accessed: 2017-10-01.

[25] Atomic force microscopy explained. https://www.nanosurf.com/en/support/afm-modes. Nanosurf, Accessed: 2017-12-20.

[26] Introduction to spectroscopy and applications. https://oceanoptics.com/wp-content/uploads/Introduction-to-Spectroscopy-and-Applications.pdf. Ocean Optics, 2017, Accessed: 2017-12-15.

[27] M.C. Schubert W. Warta T. Trupke, R.A.Bardos. Photoluminescence imaging of silicon wafers. *Appl. Phys. Lett. 89*, 2006.

[28] Jingjiao Zhang Xiaoya Ye Jianjiang Li Shuai Zou Xiadong Su Fang Cao, Kexun Chen. Quasi-steady-state photoconductance, a new method for solar cell material and device characterization. *Photovoltaic Specialists Conference, 1996, Conference Record of the Twenty Fifth IEEE*.

[29] Sinton Consulting. *WCT-120 Photoconductance Lifetime Tester and optional Suns-VOC Stage, User Manual*. 2006.

[30] Susanne Helland. Electrical characterization of amorphous silicon nitride passivation layers for crystalline silicon solar cells. *NTNU Master thesis*, june 2011.

Appendix

Sample details

Table 3: Wafer details: Siegwert Wafer

Parameter	Value [unit]
Diameter	100 ± 0.3 [mm]
Growth	Czochalski (CZ)
Doping	P-type, boron
Orientation	<100>
Thickness	275 ± 20 [µm]
Surface finish	Double Side Polished (DSP)

Table 4: Wafer details: TOPSIL

Parameter	Value [unit]
Diameter	100 ± 0.3 [mm]
Growth	FloatZone (FZ)
Doping	P-type
Orientation	<100>
Thickness	275 ± 20 [µm]
Surface finish	Double Side Polished (DSP)
Resistivity	3 ± 2 [Ω cm]

Table 5: Overview of Hole Depth Samples.

Sample	Size [mm^2]	Diameter [µm]	Distance [µm]	Etching time [s] (target depth [nm])
Sample 1	15x15	1	1	30 (150)
Sample 2	15x15	1	1	60 (300)
Sample 3	15x15	1	1	90 (450)
Sample 4	15x15	1	1	120 (600)
Sample 5	15x15	1	1	150 (750)
Sample 6	15x15	1	1	180 (900)

Table 6: Overview of Hole Width Samples.

Sample	Size [mm^2]	Diameter [µm]	Distance [µm]	Etching time [s] (target depth [nm])
Sample 1	15x15	1	1	90 (450)
Sample 2	15x15	1.5	1.5	90 (450)
Sample 3	15x15	2	2	90 (450)
Sample 4	15x15	2.5	2.5	90 (450)
Sample 5	15x15	3	3	90 (450)
Sample 6	15x15	3.5	3.5	90 (450)
Sample 7	15x15	4	4	90 (450)
Sample 8	15x15	4.5	4.5	90 (450)

Table 7: Overview of Coverage Samples.

Sample	Size [mm^2]	Diameter [µm]	Distance [µm]	Etching time [s] (target depth [nm])
Sample 1	15x15	1	0.3	90 (450)
Sample 2	15x15	1	0.5	90 (450)
Sample 3	15x15	1	0.7	90 (450)
Sample 4	15x15	1	0.9	90 (450)
Sample 5	15x15	1	1.1	90 (450)
Sample 6	15x15	1	1.3	90 (450)
Sample 7	15x15	1	1.5	90 (450)
Sample 8	15x15	1	1.7	90 (450)

Table 8: Overview of Lifetime Samples

Sample	Size [mm^2]	Diameter [µm]	Distance [µm]	Etching time [s] (target depth [nm])
Sample 1	35x35	1.5	0.7	90 (450)
Sample 2	35x35	1.5	1.5	90 (450)
Sample 3	35x35	No structure	No structure	90 (450)
Sample 4	35x35	No structure	No structure	Not etched

Dose testing

Some of the SEM images used to determine the exposure dose to use in the experiments.

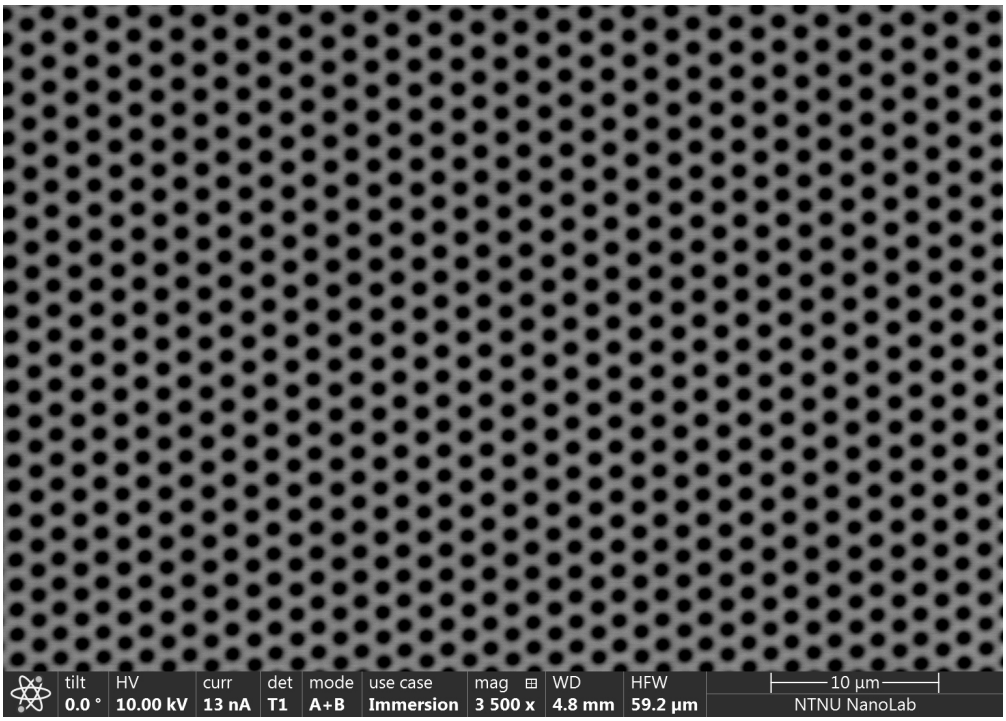

Figure 32: SEM image shows exposed and developed photoresist from a sample used to find an optimal exposure dose for the experiments. Exposure dose is 90 mJ/cm^2.

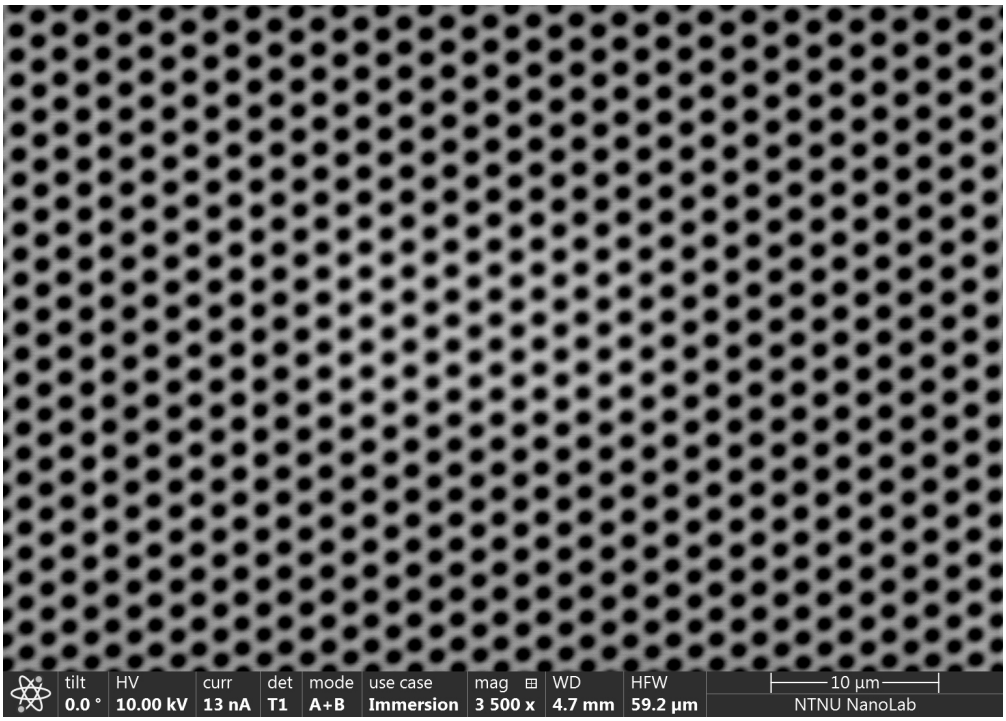

Figure 33: SEM image shows exposed and developed photoresist from a sample used to find an optimal exposure dose for the experiments. Exposure dose is 100 mJ/cm^2.

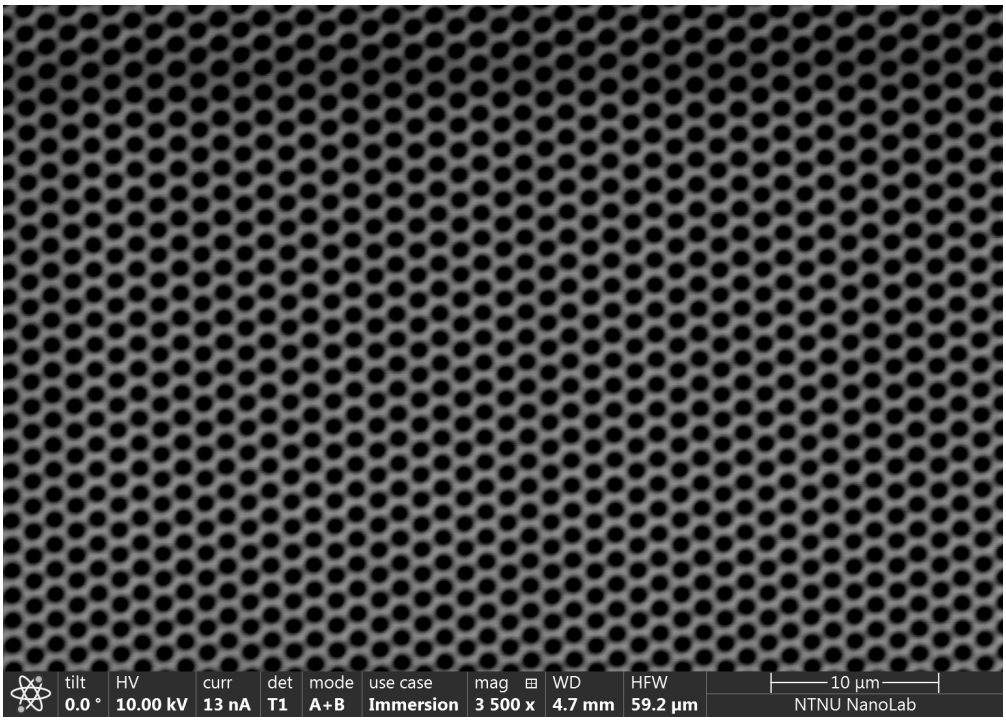

Figure 34: SEM image shows exposed and developed photoresist from a sample used to find an optimal exposure dose for the experiments. Exposure dose is 110 mJ/cm^2.

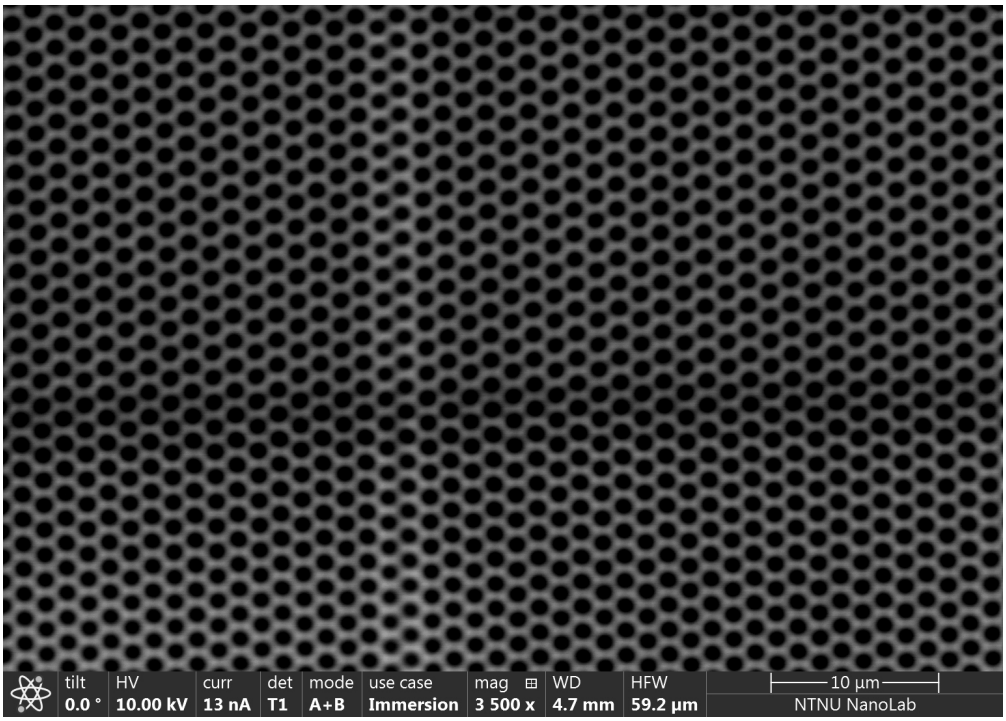

Figure 35: SEM image shows exposed and developed photoresist from a sample used to find an optimal exposure dose for the experiments. Exposure dose is 120 mJ/cm^2.

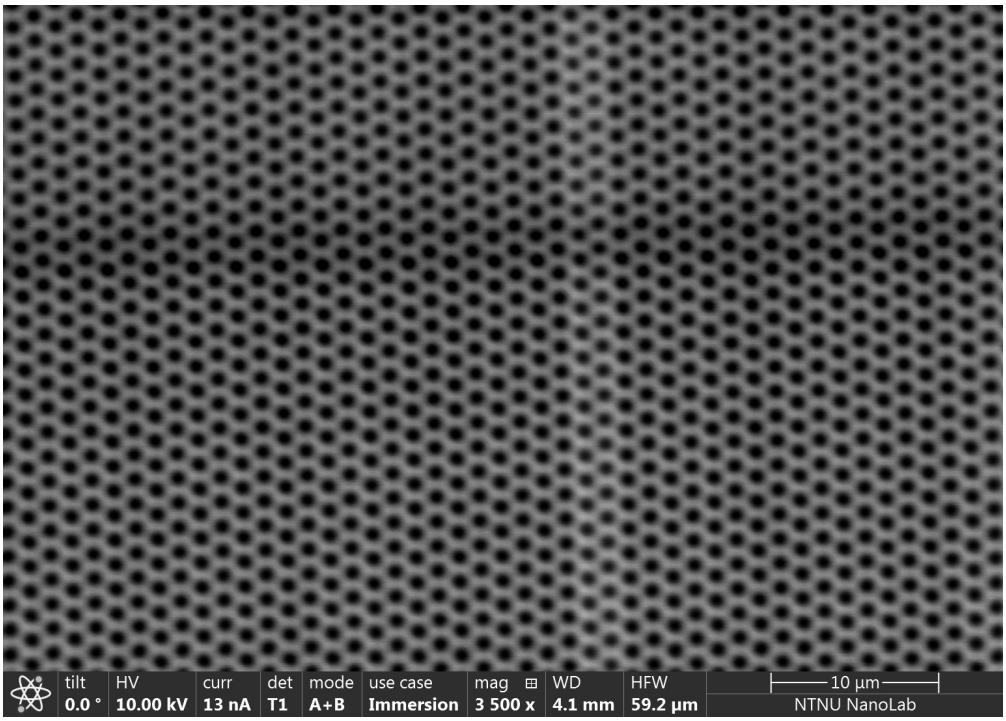

Figure 36: SEM image shows exposed and developed photoresist from a sample used to find an optimal exposure dose for the experiments. Exposure dose is 130 mJ/cm^2.

ICP-RIE details

Table 9: Detailed parameters for the ICP-RIE.

Parameter	Value [unit]
SF6	7.5 [sccm]
CHF3	50 [sccm]
Pressure	15 [mTorr]
RF power	40 [W]
ICP generator	600 [W]